Greenland glacial history, borehole constraints, and Eemian extent

L. Tarasov and W. Richard Peltier
Department of Physics, University of Toronto, Toronto, Ontario, Canada

Received 20 December 2001; revised 12 September 2002; accepted 4 October 2002; published 12 March 2003.

[1] We examine the extent to which observations from the Greenland ice sheet combined with three-dimensional dynamical ice sheet models and semi-Lagrangian tracer methods can be used to constrain inferences of the Eemian evolution of the ice sheet, of the extent and frequency of summit migration during the 100 kyr ice age cycle, and of the deep geothermal flux of heat from the Earth into the base of the ice sheet. Relative sea level, present-day surface geometry, basal temperature, and age and temperature profiles from the Greenland Ice Project (GRIP) are imposed as constraints to tune ice sheet model and climate forcing parameters. Despite the paucity of observations, model-based inferences suggest a significant northeast gradient in geothermal heat flux. Our analyses also suggest that during the glacial cycle, the contemporaneous summit only occupied the present-day location during interglacial periods. On the basis of the development and use of a high-resolution semi-Lagrangian tracer analysis methodology for $\delta^{18}O$, we rule out isotropic flow disturbances due to summit migration as a possible source of the high Eemian variability of the GRIP $\delta^{18}O$ record. Finally, in contrast with results obtained in some recent attempts to infer the extent to which Greenland may have contributed to the anomalous highstand of Eemian sea level, we find that conservative bounds for this contribution are 2–5.2 m, with a more likely range of 2.7–4.5 m. *INDEX TERMS:* 1827 Hydrology: Glaciology (1863); 1863 Hydrology: Snow and ice (1827); 3344 Meteorology and Atmospheric Dynamics: Paleoclimatology; 9315 Information Related to Geographic Region: Arctic region; *KEYWORDS:* Greenland ice sheet, Eemian, semi-Lagrangian tracer, geothermal heat flux, GRIP ice core, relative sea level

Citation: Tarasov, L., and W. R. Peltier, Greenland glacial history, borehole constraints, and Eemian extent, *J. Geophys. Res.*, *108*(B3), 2143, doi:10.1029/2001JB001731, 2003.

1. Introduction

[2] An important rational for the study of past climates is to help characterize the range of conditions that may result as a consequence of variations in the nature and strength of climate forcing. It has often been suggested that a possible analogue for the warmer climate that will characterize our future is that of the last interglacial or Eemian epoch that was centered on approximately 125 ka. The $\delta^{18}O$ records from Greenland ice cores [*Johnsen et al.*, 1997] and evidence from coral reefs [*Vezina et al.*, 1999] raise a number of important issues concerning the stability of the polar cryosphere during the Eemian period.

[3] One current issue concerns the stability of the West Antarctic Ice Sheet (WAIS). During the previous interglacial, proxy records indicate that global sea level was approximately 5 to 6 m above present level [*Vezina et al.*, 1999; *Rostami et al.*, 2000]. Therefore one or both of the existing large-scale ice sheets must have experienced significant diminution. Modeling studies have made it clear that the East Antarctic ice sheet is an unlikely source for the excess sea level contribution [*Huybrechts*, 1994], as increased snow accumulation tends to offset the impact of increased ablation for warming of order 5°C or less relative to present climate. The status of the WAIS is less clear. Modeling studies suggest that the WAIS is in an unstable equilibrium, and surging ice streams could possibly destabilize a large portion of this ice sheet [*Huybrechts*, 1990].

[4] One possible way to constrain the stability of the WAIS is to bound the contribution from the remaining large-scale ice sheet, i.e., that situated on Greenland. A recent model-based analysis of the Greenland ice sheet [*Cuffey and Marshall*, 2000] based upon revised $\delta^{18}O$ paleothermometric calibrations has argued for a much stronger Eemian deglaciation of Greenland than previously assumed, with a greater than 4 m contribution to excess Eemian sea level rise deemed the most likely scenario. Given the relatively weak observational constraints on current three-dimensional (3-D) models of the Greenland ice sheet along with significant uncertainties associated with the paleothermometric calibration, assumed atmospheric lapse rate (upon which the $\delta^{18}O$ to climate forcing inversion depends), and the assumed Greenland Ice Project (GRIP) (i.e., summit) site ice source elevation used in the above analyses, an independent reexamination of the Eemian Greenland sea level contribution using a more complete approach to constraining the model is warranted. One goal of the present paper is to present such a reexamination.

0148-0227/03/2001JB001731$09.00

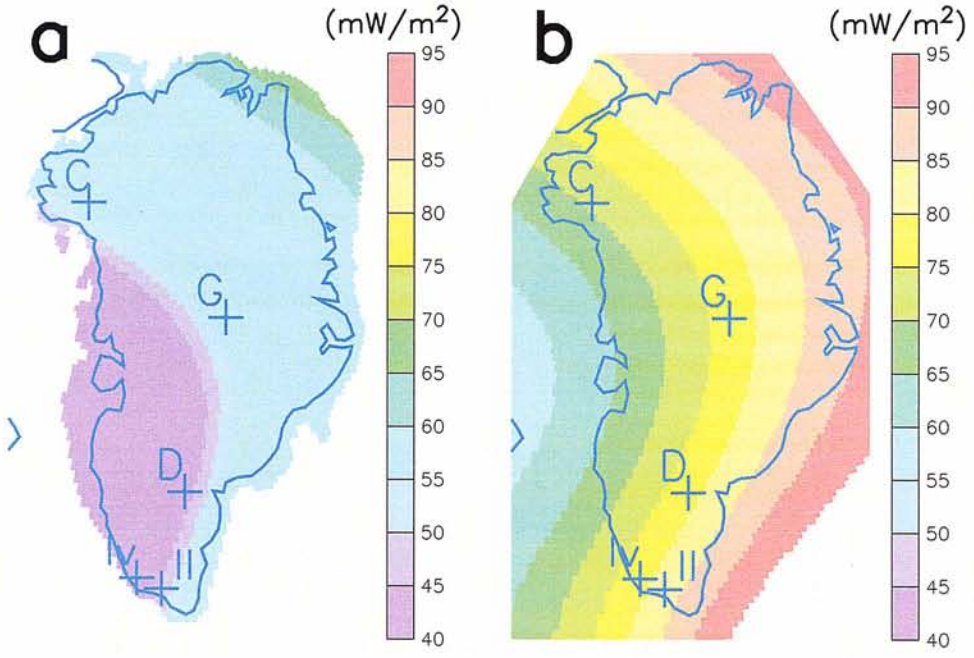

Figure 6. (a) New and (b) *Pollack et al.* [1993] geothermal heat flux maps with GRIP (G), Camp Century (C), Dye 3 (D), Ivigtut (Iv), and Ilimaussaq (ll) sites indicated.

[46] Basal temperature at summit is quite sensitive to the deep geothermal heat flux. In the neighborhood of 50 mW m^{-2}, a 1 mW m^{-2} change in the heat flux will result in a 0.4°C change in present-day modeled basal temperature. We obtained a very close fit to the observed borehole temperature profile at GRIP shown in Figure 7 by using the new heat flux map which has a geothermal heat flux value of 57.56 mW m^{-2} below summit. The only discrepancies between the prediction of the tuned model and the observed temperature profile occur at the top and bottom of the core. At the top, the model profile has an insufficient and too near surface Little Ice Age cold bump arising at least in part from the lack of accounting for firn densification processes which are observed to be significant for approximately the top 100m. At the bottom, model basal temperature is 0.7°C too cold as compared to observations. This discrepancy was unavoidable in order to best fit the observed temperature profile. The geothermal heat flux required for our model is significantly above the median value of 51.3 mW m^{-2} required to obtain a close fit in the 1-D Monte Carlo inversion of the observed borehole temperature profile at GRIP by *Dahl-Jensen et al.* [1998]. Furthermore, this latter inversion also used a higher accumulation rate, which would have increased downward cold advection compared to model GrB and thus even further depressed basal temperature.

[47] This geothermal heat flux discrepancy between 1-D and 3-D modeling is due to a combination of at least four factors. First, the 3-D GrB model is tuned to match the present-day surface elevation at summit, but this does not allow for an exact match of present-day ice thickness. The model underpredicts the ice thickness at summit by 3029 − 2963 = 66 m. Extrapolation of the near basal temperature profile to the observed ice depth at GRIP results in a basal temperature 1.1°C too warm. Second, the vertical resolution of the model introduces some inaccuracies. A doubling of vertical resolution to 130 layers, does result in a slightly warmer base (−9.09°C) due to better resolution of both near-basal strain and the vertical temperature gradient. However, further doubling (−9.01°C) and extrapolation to an infinite number of levels gives −8.9°C. Neglecting the need for retuning of other model parameters, the above two factors account for about a 1.4°C/0.4 mW m^{-2} per °C or 3.5 mW m^{-2} reduction in the geothermal heat flux discrepancy.

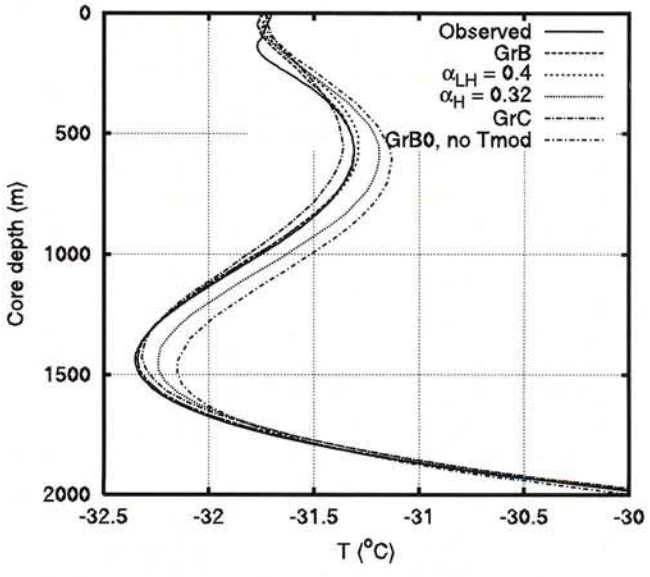

Figure 7. GRIP borehole temperature profile sensitivity to variations of α_c (Holocene (H) and last 1 kyr (LH)), for GrB model without near margin Holocene temperature forcing adjustments (No Tmod), and for model GrC using α_c from 1-D model-based borehole temperature inversion of *Cuffey and Clow* [1997].

[48] The remaining approximately 3 mW m^{-2} discrepancy between 1-D and 3-D models is likely due to some combination of the lack of accounting for the impact of longitudinal stress deviations and the limitations of 1-D models. The latter must ignore horizontal heat advection, assume a poorly constrained surface elevation chronology, and also must assume negligible impact from the displacement of summit over the glacial cycle. As will be discussed below, the model summit is located within the grid cell corresponding to the present-day summit only during parts of interglacials and never during glacial periods.

[49] By adjusting glacial, Holocene, and late Holocene values of α_c (see Table 1), we have obtained a close match to the observed borehole temperature profile at GRIP, with the only discernible discrepancy near the surface, possibly due to the lack of accounting of low-density firn layers. Also shown in Figure 7 is the resultant present-day borehole temperature profile for the untuned model GrB0 (only tuned to maximum surface elevation) and for models with modified α_{cLH} (late Holocene) and α_c(Holocene). It should be clear that the close fit in borehole temperature profile achieved is a nontrivial constraint on the model.

[50] We have also retuned the model to use the best fit climatic isotopic parameters of *Cuffey and Clow* [1997] derived by 1-D model-based inversion of the GISPII borehole temperature profile. Following their model tuning, we also added a dynamic precipitation-scale correction (applied everywhere) to ensure agreement between model and inferred accumulation history at the GISPII site. With a 1.5 mW m^{-2} reduction in the model geothermal heat flux (which gives a value of 56 mW m^{-2} at GRIP) and an increase in the flow enhancement parameter from 5.1 to 6.0, this new model ("GrC") also delivers a reasonably close fit to the observed borehole temperature profile at GRIP as shown in Figure 7. Given the significant difference in Holocene climatic isotopic parameters between model GrB and that of *Cuffey and Clow* [1997] (0.364 and 0.25, respectively), it is therefore clear that the GRIP borehole temperature profile alone provides only a limited constraint on inferred climate.

[51] As an independent test, it is worth examining other borehole temperature profiles (which were not employed to tune the model). Model GrB somewhat misfits the borehole temperature profile at the GISP II site as shown in Figure 8. Whether this is a consequence of limited model resolution, lack of accounting for the impact of longitudinal stresses on ice flow, inappropriate ice rheology, insufficient surface gradient in climate, or significant discrepancies in the transient evolution of the ice sheet geometry is unclear. This result clearly requires that we acknowledge the limitations of current state-of-the-art 3-D ice sheet models that rely on simplified climate forcing. The predicted borehole temperature profile for the new NGRIP site is also shown in Figure 8. In comparison to the GRIP borehole profile, GrB NGRIP is distinguished by a 63% stronger glacial cold peak and a 30% weaker Holocene warm peak along with a 1.74°C warmer basal temperature (−7.5°). Observationally based inferences indicate that the base of NGRIP is near the pressure melting point, at about −2.5°C (D. Dahl-Jensen, personal communication, 2002) which is thus much warmer than the model prediction. Extrapolation of model temperature to the NGRIP site depth of 3100 m gives a temperature of −2.5 °C for the NGRIP grid cell. Thus the discrepancy in basal temperature is largely if not entirely due to the approximately 170 m thinner ice in the model NGRIP grid cell. The weaker Holocene warm peak is due to the continuous Holocene high surface elevation of the model NGRIP site in contradistinction to the model GRIP site which experiences a mid-Holocene elevation depression of about 140m. During the glacial period, model NGRIP and GRIP site elevation changes were generally quite similar and therefore the colder glacial peak in the NGRIP temperature profile is largely if not solely due to the increasing impact with depth of advected cold ice from higher elevations.

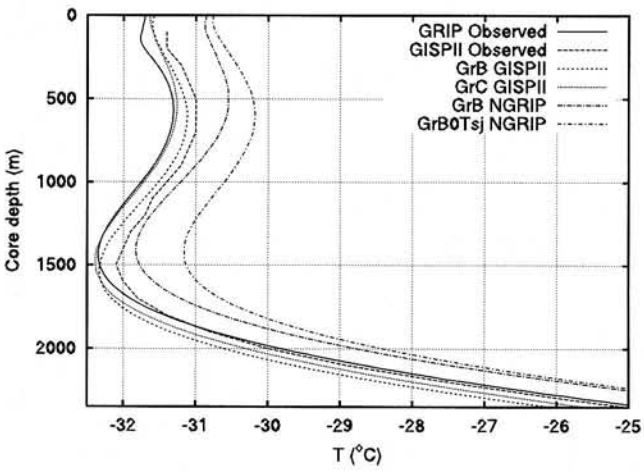

Figure 8. Borehole temperature profile comparisons for GRIP, GISP II, and NGRIP. GISP II model value has been interpolated to a location matching the relational positioning of the GRIP and GISP II sites.

3.2. Constraints on the Eemian Evolution of the Greenland Ice Sheet

[52] Having described the model and the quality of the fit to the imposed constraints, we will next proceed to use the model to investigate Summit migration, $\delta^{18}O$ tracer predictions, and the constraint on Eemian Greenland ice sheet evolution.

3.2.1. Summit Migration and Ice Source Elevation

[53] As 1-D inversions of both the borehole temperature and age profiles at GRIP rely on the assumption of a stationary summit, it is an important check to consider the summit location chronology of tuned 3-D models. As shown in Figure 9, model GrB summit position matches the current location only during the latter parts of interglacials. During glacial periods, the model summit is located a quarter to half a degree to the south and oscillates a half degree (single grid point distance) to the west. This single grid point oscillation may arise solely from the limited numerical resolution. *Marshall and Cuffey* [2000] find a somewhat similar pattern of summit migration, although with approximately twice the migration distance. As noted by *Marshall and Cuffey* [2000], such summit displacement can explain the absence of an observed bump in isochronal

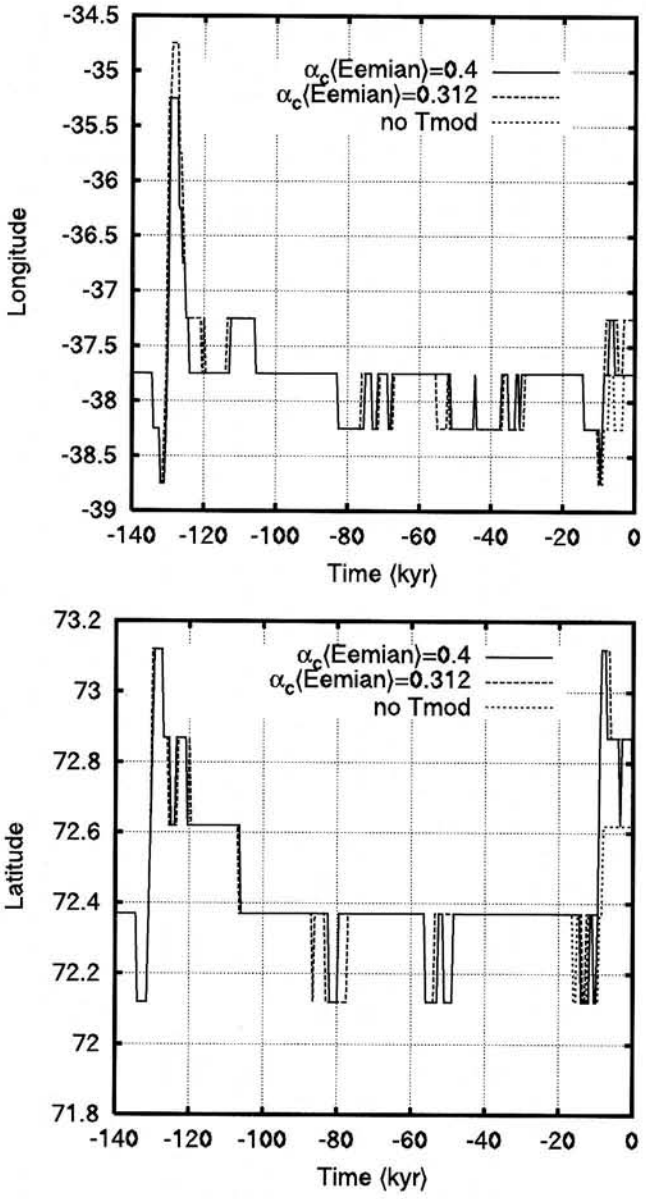

Figure 9. Greenland summit location chronology for different values of the Eemian isotopic sensitivity (α_c) and for the model without regional Holocene temperature forcing modifications (no Tmod).

layers ("Raymond bump" [*Raymond*, 1983]) under summit which is expected for the case of a stationary summit [e.g., *Schott-Hvidberg et al.*, 1997].

[54] The cyclical displacement of summit also implies that much of the ice in the GRIP ice core did not originate from that location. Given the $\delta^{18}O$ to temperature dependence on elevation, ice source elevation needs to be explicitly taken into account in deriving a climate forcing from the GRIP $\delta^{18}O$ record. We have traced ice source elevation back to the Eemian optimal. Furthermore, to eliminate the influence of the assumption that the ice was sourced from the time-dependent elevation of the GRIP site, we have twice iterated model runs with ice source elevation chronologies from previous runs (we employed the ratio of the source elevation minus GRIP elevation to the difference between the contemporaneous summit elevation and the GRIP elevation to fix the source elevation history for the next iteration). From approximately 70 ka until present, ice originated from very close to the GRIP site as shown in Figure 10. Further back in time, source elevation varies away from that of the contemporaneous GRIP site, bounded of course by the elevation of summit and of the GRIP site (though numerical dissipation in the tracer model occasionally oversteps these bounds). The difference in elevation between summit and the GRIP site remains small until the Eemian. Most important for constraining the Eemian minimum of the Greenland ice mass, source elevation during the Eemian minimum is effectively that of GRIP which is significantly below the contemporaneous modeled summit. This will have a significant impact on the magnitude of the contribution inferred for the Greenland ice sheet to the Eemian sea level highstand (see below).

3.2.2. $\delta^{18}O$ Tracer Analyses

[55] It has remained somewhat contentious concerning the extent to which the Eemian section of the GRIP ice core has suffered flow/fabric disturbances and therefore disturbances to the inferred $\delta^{18}O$ chronologies [*Johnsen et al.*, 1997]. The profiles of certain chemical tracers across the sudden apparent cooling events of the Eemian are difficult to explain if these events were the result of stratigraphic disturbances [*Steffensen et al.*, 1997]. Records from the subpolar North Atlantic suggest that coupled surface-deepwater oscillations occurred just prior to the Eemian interglacial [*Oppo et al.*, 2001]. There is also some far-field evidence from Lake Baikal biogenic silica and microfossil abundance records for a mid-Eemian cooling event [*Karabanov et al.*, 2000]. On the other hand, the methane variations across the Eemian segment of the GRIP and GISPII cores has no counterpart in the Vostok record, suggesting that there is stratigraphic disturbance [*Chappellaz et al.*, 1997]. On the basis of the apparently much more stable Eemian Antarctic climate, *Cuffey and*

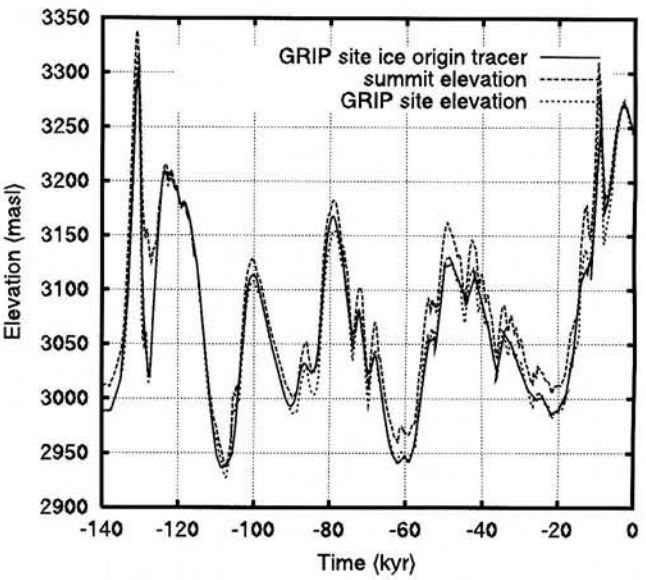

Figure 10. Surface elevation chronology of contemporaneous regional summit, GRIP, and GRIP site ice source.

Marshall [2000] argue that the Vostok Deuterium record provides a more realistic chronology for the period prior to 100 ka. We have followed their suggestion in splicing the Vostok chronology onto the Greenland record with extremal amplitude adjusted to that of the GRIP record. However, this is problematic in that matching of the extremal amplitude from the last 250 kyr (see the reconstruction labeled DVw in Figure 11) results in a significantly different reconstruction as opposed to matching for the period prior to 105 ka (reconstruction DV). Unless otherwise specified, we will therefore use the DV chronology for subsequent analyses.

[56] The synthetic GRIP $\delta^{18}O$ profiles obtained in this way have an excellent match with observations for the glacial period back to just prior to the Eemian as is evident in Figure 12, further validating the quality of the tuned model. However, during the Eemian and also for the period after last glacial maximum, phase differences indicate limitations in the model ice sheet chronology. For this latter period, downward displacement of the phase profile indicates excessive ice accumulation at the start of the Holocene period. This is likely a result of the computationally convenient assumption of thermodynamic control on temporal precipitation change which holds reasonably well for glacial periods. This assumption has been shown not to hold for the early Holocene for which changes in atmospheric circulation appear to dominate temporal changes in precipitation [*Cuffey and Clow*, 1997]. For the mid-Eemian period, the phase error of the model $\delta^{18}O$ profile is opposite to that of the early Holocene (Figure 12). This is again likely due to the impact of atmospheric circulation changes on the regional accumulation rate. However, at this depth, we cannot rule out that some phase error may also be arising from limitations of the ice flow chronology, possibly due to the lack of accounting for longitudinal stresses or differences in the evolved geometry of the ice sheet.

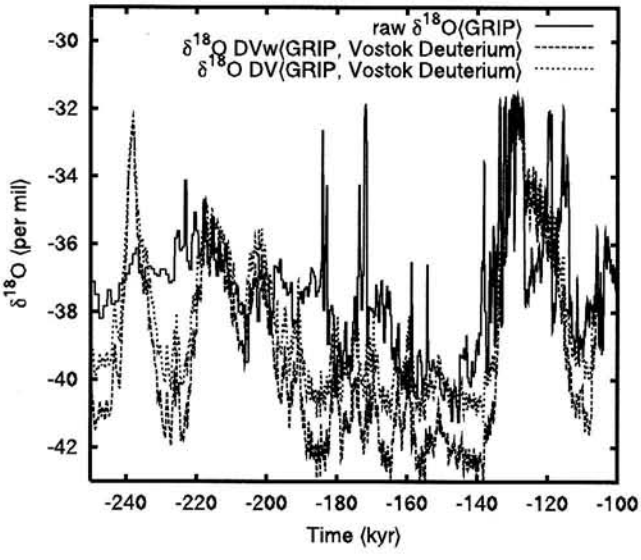

Figure 11. Modified $\delta^{18}O$ input chronologies. Chronology DV uses the Vostok deuterium chronology for the period prior to 105 ka with amplitude and mean adjusted so that extremal $\delta^{18}O$ values for that period match those of the raw GRIP record. DVw is similar, except that the extremal match is over the whole length of the GRIP recorded. The $\delta^{18}O$(GRIP) is from *World Data Center A for Paleoclimatology* [1997].

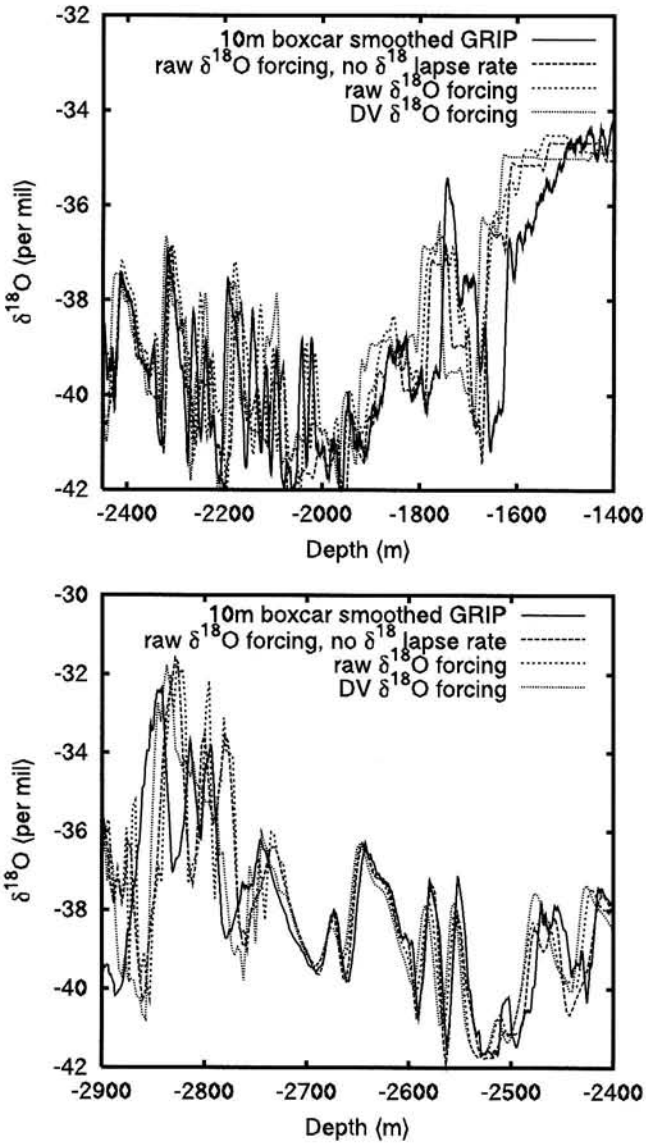

Figure 12. Observed and model $\delta^{18}O$ profiles at GRIP site. Model profiles based on $\delta^{18}O$ forcings using both the raw $\delta^{18}O$ GRIP chronology and the DV (refer to text) $\delta^{18}O$ chronology based on the Vostok Deuterium excess chronology for pre-105 ka. Also shown are results for $\delta^{18}O$ forcing without the $\delta^{18}O$ lapse rate.

[57] The impact of the assumed $\delta^{18}O$ lapse rate on the inferred time series of surface $\delta^{18}O$ variations that is required to drive the tracer model is small relative to other sources of uncertainty and tends to consist of a slight shift to higher values of the downcore $\delta^{18}O$ values relative to those predicted without adjustment of the lapse rate effect. It must be remembered that the source elevations employed for the $\delta^{18}O$ inversion are obtained by iterated tracing of ice source location for the model GRIP core. The impact of the assumed $\delta^{18}O$ lapse rate on sites further from summit will likely be larger.

[58] Validation of the tuned coupled model and of the tracer module allows a clear test of a possible source of the high Eemian variability of the GRIP $\delta^{18}O$ record. Comparison of the Eemian profiles for models driven with the raw GRIP $\delta^{18}O$ chronology and the DV $\delta^{18}O$ chronology with much lower Eemian variability in Figure 12 shows that with an isotropic flow law model that ignores longitudinal stresses, there is no discernible contribution to $\delta^{18}O$ Eemian variability arising from model summit migration. Therefore, it is likely that the main source of flow disturbance to the Eemian segment of the GRIP $\delta^{18}O$ record is due to dynamically induced folding of the stratigraphy arising from anisotropic components of the ice rheology [*Dahl-Jensen et al.*, 1997].

[59] We have also examined whether the $\delta^{18}O$ record could be used to constrain the Eemian $\delta^{18}O$ sensitivity to temperature and thereby indirectly Eemian extent. However, we find no significant difference in the GRIP site $\delta^{18}O$ tracer record for models using 0.312 and 0.5 values of α_c for the Eemian period.

[60] While the tracer $\delta^{18}O$ profile for the GRIP site has significant phase errors only during the interglacial and terminal glacial periods, the tracer profile for the GISP II site (Figure 13) displays excessive downward phase displacement throughout the core. The GISPII record is indeed displaced downward during the glacial period relative to the GRIP core, but not as much as the tracer model predicts. The tracer $\delta^{18}O$ chronologies for the GRIP and GISPII sites are very similar and the GISPII site tracer is closer to the inferred GRIP record than to the inferred GISPII record (not shown), indicating the spatial persistence of the forcing chronology when using such a simple $\delta^{18}O$ forcing for the ice sheet.

[61] The $\delta^{18}O$ tracer chronology for the NGRIP site is displaced upward by about 2.1 per mil relative to that for the GRIP site (Figure 14). This is a direct result of the 344 m difference in present-day surface elevation between the two model sites and the $\delta^{18}O$ lapse rate used to compute the upper boundary condition for the tracer. Aside from this bias, the $\delta^{18}O$ tracer for NGRIP closely follows the GRIP record with a cold (increasing isotopic depletion) drift toward the Eemian arising from the nearer to summit sourcing of the older (i.e., deeper) ice. It is also worth noting the significantly reduced signal dissipation at the NGRIP site that most likely arises from a longer projected horizontal relative wavelength due to a stronger and more horizontal flow. Further improvements in signal quality will likely arise further downstream until the vertical component of the ice flow starts to increase near the margins. This would benefit possible future studies combining advanced $\delta^{18}O$ deposition models with coupled ice sheet tracer models. Comparison of model and far from summit ice core $\delta^{18}O$ profiles could offer powerful constraints on the transient history of existing ice sheets.

3.2.3. Eemian Sea Level Contribution

[62] Crucial to constraining the minimum volume of the Greenland ice sheet during the Eemian interglacial is the representation of climate forcing assumed in the analysis, or in this case the $\delta^{18}O$ paleothermometric calibration. If we were to assume that α_c(Holocene) is close to α_c(Eemian), the difference in α_c(Holocene) between models GrB and GrC

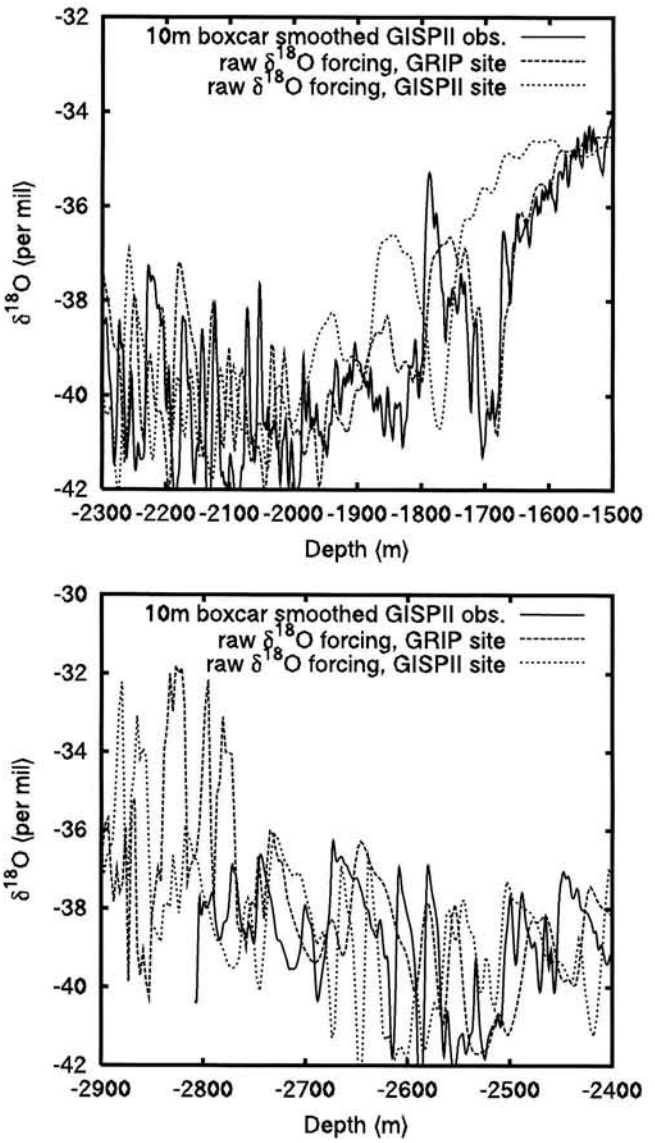

Figure 13. Observed and model $\delta^{18}O$ profiles at the GISP II and GRIP site using the raw GRIP $\delta^{18}O$ forcing with $\delta^{18}O$ lapse rate.

(both of which fit the GRIP borehole temperature and inferred age profiles) already implies significant uncertainty in the inferred Eemian climate. Furthermore, a more complete probe of parameter space would likely offer an even larger range in possible values of α_c(Holocene). Other independent constraints on α_c would therefore be useful.

[63] A number of processes are likely involved in determining the value of α_c [*Cuffey*, 2000]. One-dimensional model-based analyses, for instance, suggest that changes in source temperature and regional evaporative recharge rates can alone explain the difference between observed spatial gradients of $\delta^{18}O$ (with respect to temperature) and inferred temporal gradients for the Antarctic [*Hendricks et al.*, 2000]. A different physical basis for the small value of α_{cG} (during the glacial period) in comparison to the present-day value inferred on the basis of

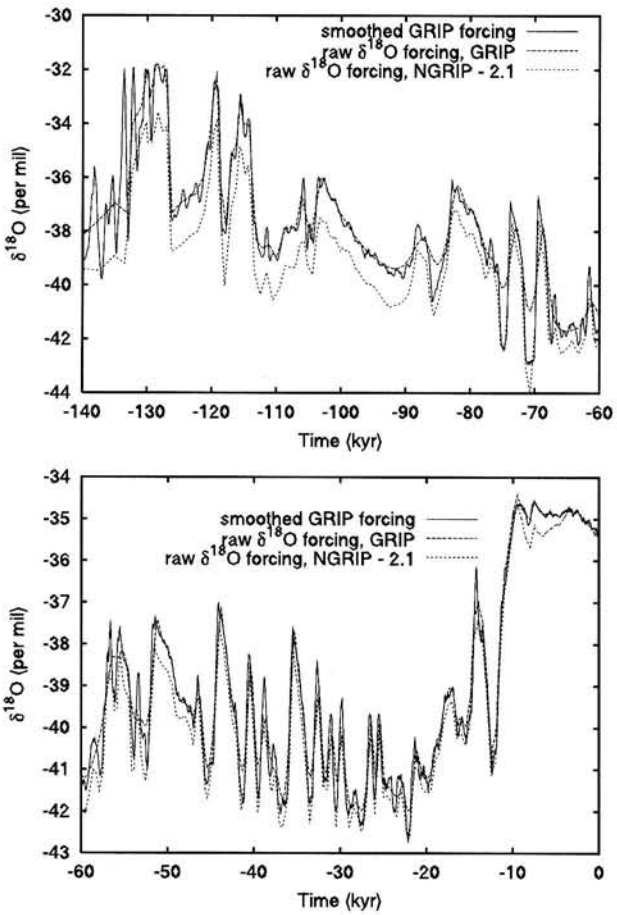

Figure 14. $\delta^{18}O$ chronology for GRIP and NGRIP using the raw GRIP $\delta^{18}O$ forcing with $\delta^{18}O$ lapse rate.

observed spatial and temporal isotopic gradients has been suggested by AGCM-based analyses [*Fawcett et al.*, 1997; *Krinner et al.*, 1997; *Werner et al.*, 2000]. A reduction in α_c from the warm Holocene to the cold glacial is attributed to the increased seasonality of precipitation during glacial periods with little accompanying change in the temporal form of the seasonal cycle of either the surface temperature or $\delta^{18}O$. The $\delta^{18}O$ record thus becomes a more warm-biased temperature proxy during glacial times. Other possible contributing factors, such as changes in the origin of precipitation and changes in tropical sea surface temperatures, have been found to be much less important in AGCM studies [*Werner et al.*, 2000]. While an increase in present-day mean temperature could further reduce the seasonality of precipitation, the rate at which this takes place as a function of temperature change is likely to be much less than for colder climates. For glacial climate, GCM simulations indicate a much more zonal winter circulation which drastically reduces the transport of moisture to the ice sheet [*Werner et al.*, 2000]. There is no direct evidence nor any apparent physical basis for suggesting a similar change in atmospheric circulation with warmer climates typical of the mid-Holocene or Eemian. The impact of changes to ocean water $\delta^{18}O$ will also be much smaller for warmer than present as compared to colder than present climates. In contradiction therefore to recent 1-D model-based borehole temperature inversions for the Holocene period, one would expect α_c for periods warmer than present to be no smaller than that for present-day and to also be larger than α_{cG}. Therefore, we base our upper bound for α_c(Eemian) on the present-day bound for α_c. *Shuman et al.* [1998] have measured the present-day (seasonally based) value of α_c to be most likely between 0.4 and 0.5, with 95% confidence intervals of 0.34 to 0.68 [*Shuman et al.*, 1995]. The 1-D model-based borehole temperature inversion of *Cuffey et al.* [1995] also required a value of α_c of 0.47 for the last 500 years. The older and more poorly fitting paleothermometric calibration of *Johnsen et al.* [1989] has an α_c value of 0.6 for high $\delta^{18}O$ values that characterize the Holocene. Given the ranges of these previous analyses, we choose a value of 0.6 as a defensible upper bound for α_c(Eemian).

[64] As a lower bound for plausible values of α_c(Eemian), we initially choose the value of α_c(Holocene) = 0.25 from the analyses of *Cuffey and Clow* [1997]. Rerunning the constrained model using this range of Eemian α_c, we obtain a range of minimum ice volumes from 2.23 to 1.12×10^{15} m^3 for model GrB when the Vostok DV $\delta^{18}O$ chronology is assumed. Extracting sea level contributions is further complicated by the 7% excess present-day ice volume in the model. Figure 15 presents estimated eustatic sea level contributions reduced by the ratio of the present-day excess model volume (i.e., by 1/1.07).

[65] On the basis of the total gas content record of the GRIP core [*Raynaud et al.*, 1997], *Cuffey and Marshall* [2000] argue that the minimum Eemian elevation of the GRIP core ice was no lower than about 2900 m. As indicated by the boxes in Figure 15, this provides an upper bound to maximum Eemian sea level contributions of about 4.4 m and 3.9 m, respectively, for model GrB with accounting for GRIP ice source elevation and model GrC (without such accounting). Lower bounds for the models are near 2 m. Different model precipitation sensitivities to temperature change likely accounts for the model tuned with the low value of α_c(Holocene) (=0.25, GrC) also having the lowest sea level contribution for the lower boundary value of α_c(Eemian). The significantly different slope of the GrC sea level sensitivity curve suggests even further caution in interpreting model-based constraints upon the volume of the Greenland ice sheet during the Eemian interglacial.

[66] One way in which we might better quantify the impact of the entire set of constraints employed to construct model GrB is to compare the sea level sensitivity curve for the untuned version of GrB (Figure 15, "untuned model", with DV $\delta^{18}O$ chronology) to that for the fully tuned model. This "untuned" model was only tuned to approximate present-day ice volume and elevation at summit (using only flow enhancement and sliding parameters). RSL dates, present-day topography, and borehole temperature and age profile constraints were thereby ignored. This relatively unconstrained model predicts approximately an extra 0.5 m of excess Eemian sea level contribution arising from the prolonged period of high climate variability.

[67] While the predicted Eemian sea level excess for Greenland is most sensitive to the assumed value for Eemian isotopic sensitivity other factors are not insignif-

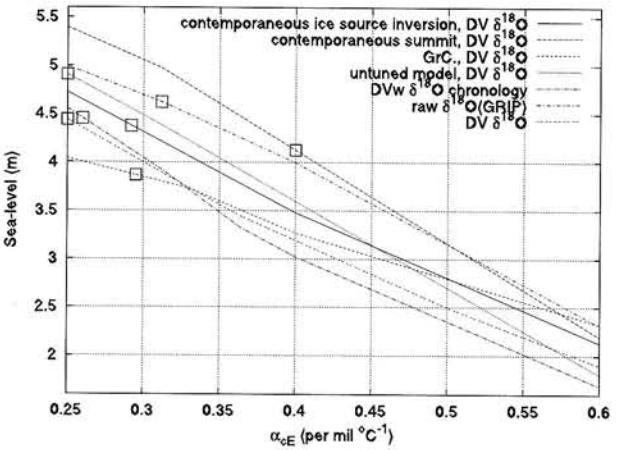

Figure 15. Eemian excess sea level contribution from Greenland as a function of α_c, $\delta^{18}O$ chronology, and assumed ice source location for the GRIP record. "Contemporaneous ice source inversion" uses iterated runs to obtain a self-consistent source elevation for the GRIP ice used in the $\delta^{18}O$ to temperature transfer function/forcing. "Contemporaneous summit" assumes that GRIP ice is sourced from the contemporaneous summit. $\delta^{18}O$ chronologies are as indicated (refer to text and Figure 11 for details).

icant. Use of the $\delta^{18}O$ chronology with high Eemian variability (i.e., the unmodified GRIP record) for the climate forcing results in an extra 0.6 to 0.7 m sea level contribution. Given its dependence upon the vagaries of midlatitude storm track migration, it is likely that the true Eemian Greenland climate resides somewhere between the extremes represented by the GRIP and Vostok DV chronologies. The assumed source elevation of the GRIP site ice is also important. The assumption of GRIP ice sourced to the contemporaneous summit can result in more than a meter of extra sea level contribution as compared to the assumption of locally sourced ice and more than 0.7 m excess relative to models that take into account the actual (model) source elevation of the GRIP site ice.

[68] One additional uncertainty requires consideration. As detailed by *Tarasov and Peltier* [2002], our model of Greenland ice sheet evolution required significant modifications to the near coastal Holocene temperature forcing in order to match computed and observed relative sea level observations. We suspect that a significant fraction of this extra forcing is accounting for the lack of explicit fast flow mechanics in the ice sheet model. Whatever this extra forcing represents, the apparent need for this enhanced forcing during the Holocene would suggest that the deglaciation event predicted under the assumption of a simple climate forcing based upon a single proxy may well underrepresent the diminution of ice volume that actually occurred during the Eemian. During the Holocene minimum at 8.5 ka, differences in ice volume between the fully tuned model and the model lacking the modified Holocene regional temperature forcing were $3.205 \times 10^{15} - 2.925 \times 10^{15} = 0.28 \times 10^{15}$ m^3. Subsequent to this, differences diminished. If we simply take this as an additional uncertainty in our estimation of the maximal excess Eemian sea level contribution, this adds 0.7 m of possible additional sea level contribution.

[69] Most problematic is the reliance on a single climate proxy from the summit of Greenland to derive a climate chronology for the whole of Greenland. Recent observations find anticorrelations between local climatic responses for the east and west coastal regions [*White et al.*, 1997]. Yet it is precisely the near-margin climate that will largely determine the extent of Greenland ice. The apparent absence of deep water formation in the Labrador Sea during the Eemian interglacial [*Hillaire-Marcel et al.*, 2001] would have limited oceanic heat transfer to the region, suggesting limited regional warming. On the other hand, this situation might have been caused by a large freshwater flux from Greenland, suggesting fast and significant deglaciation. It is therefore important to investigate other possible constraints on the extent of Eemian Greenland deglaciation.

[70] Inferences on the marginal extent of the Eemian Greenland ice sheet might be obtained from ice cores located in regions that were potentially deglaciated during the Eemian. Considering Camp Century and Dye 3, for instance, Camp Century retains ice even for α_c(Eemian) = 0.312 (Figure 16), while Dye 3 is barely covered by the margin of a residual dome for α_c(Eemian) = 0.6 and is fully deglaciated with α_c(Eemian) = 0.5. For all cases, the southern dome is cutoff from the rest of the ice sheet at the time of minimal Eemian extent, in contrast to the Holocene minimal extent at −8 kyr. In the model, the ice divide upon which Camp Century resides is much more robust against Eemian warming than the southern dome upon which Dye 3 resides. *Koerner* [1989] presents some evidence for Eemian ice-free conditions at both Dye 3 and Camp Century but no definitive conclusion. If observations could provide strong independent evidence for bedrock exposure at Camp Century during the Eemian, this would tend to imply a very strong Eemian deglaciation and a much warmer climate. On the other hand, our analyses do suggest that Dye 3 was ice-free during the Eemian.

[71] Independent observational constraints on Eemian climate are generally lacking. However, macrofossil analyses of a till-covered sequence in Washington Land, northwestern Greenland [*Bennike and Jepsen*, 2000], suggests that the Eemian interglacial climate was not too different from modern. Given that the regional sea level adjusted warming during the peak of the Eemian is a significant 6.8°C relative to present-day for α_c(Eemian) = 0.4, this data favors a larger value of α_c(Eemian) (and therefore limited warming).

[72] The above model results and observations suggest that a reasonable upper bound for Eemian Greenland eustatic sea level contribution is about 5.2 m (2900 m GRIP Eemian elevation limit for model GrB, with contemporaneous ice source inversion plus 0.7 m uncertainty arising from Holocene model tuning as discussed above), while a lower bound is no more than 2 m. However, given the numerous sources of uncertainty, even wider bounds are possible. More likely values are arguably bounded by α_c(Eemian) = α_c(Holocene) (or α_c(Eemian) corresponding to 2900 m minimum GRIP site elevation, whichever con-

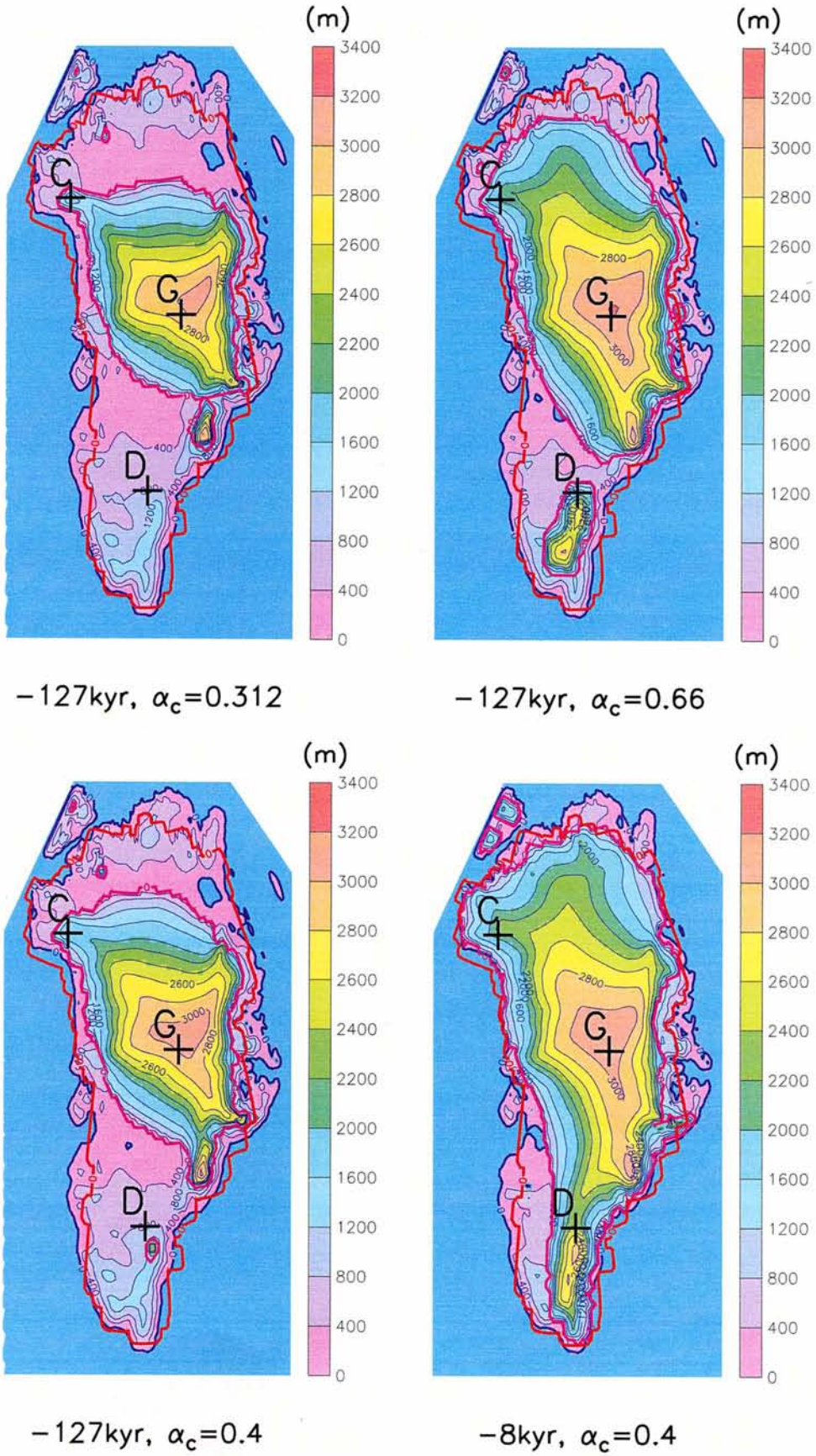

Figure 16. Eemian minimal extent for different contemporaneous climate forcings as well as minimal Holocene extent. Present-day observed ice margin (red) and contemporaneous modeled ice margin (violet) and Camp Century (C), Dye 3 (D) and GRIP (G) sites are also shown.

straint is stronger) and by the present-day observed value of α_c of approximately 0.5. This corresponds to a range of about 2.7 m to 4.5 m for the set of models GrB and GrC (with 0.6 extra meters added to GrC to allow for source elevation discrepancies and regional variations in climate). This contrasts with the 4 to 5.5 m likely range estimate of *Cuffey and Marshall* [2000], who use a stricter upper bound for α_c(Eemian) of 0.43 based on central Greenland borehole temperature analyses from the last 5 kyr and who set their lower bound to the 2900 m elevation constraint. Some of the range difference is also due to different model sensitivities and assumed contemporaneous summit sourcing of GRIP ice (though Cuffey has indicated that their model has low sensitivity to assumed ice source location (K. M. Cuffey, personal communication, 2001)). For instance, at α_c(Eemian) = 0.36, model GrB (DV δ^{18}O chronology) has Eemian sea level contributions of 3.8 m and 4.5 m for respectively source-traced and summit-traced ice, while *Cuffey and Marshall* [2000] have almost a 5 m contribution using summit-traced ice. This increased Eemian deglaciation is likely due to the stronger slope-dependent feedback in the precipitation factor that *Cuffey and Marshall* [2000] employed which tends to reduce summit elevation changes and thereby allow stronger inferred climate changes for a given α_c(Eemian) (refer to equation (6)). In order to match borehole temperature and age profiles for the GRIP site, we found it necessary to weaken the slope-dependent factor for higher elevations (equation (5)). Given the more complete set of constraints imposed upon the model, our results suggest that the 5–6 m excess eustatic rise generally assumed to characterize the penultimate interglacial [e.g., see *Rostami et al.*, 2000] likely also involved mass loss from the south polar cryosphere.

4. Conclusions

[73] In comparison to previous modeling studies of the Greenland ice sheet, we have imposed a number of new constraints on its evolution as described herein. Precipitation sensitivity to climate forcing and geothermal heat flux were adjusted in order to obtain a close fit with the observed borehole temperature and age profile at GRIP, to provide approximate matches to recorded basal temperature observations at Dye 3 and Camp Century and to produce an accumulation history that is bounded by inferences from the GRIP and GISP II ice cores. In so doing, we thereby also provide 3-D modeling corroboration of the significantly reduced temporal isotopic gradient (α_c) relative to the observed spatial gradient, especially for glacial climates. Obtaining model correspondence to RSL observations required further regional modifications to calving and precipitation sensitivity parameters. Further ad hoc regional Holocene temperature forcings were also required to fit the observations, attesting to the nontrivial nature of the complete set of constraints.

[74] Comparisons against other ice core data allowed independent tests of the constrained model. Limitations of the model were apparent in the weaker model correspondence to the temperature profile at the GISP II site. This discrepancy may arise from inaccuracies in the input basal and surface topographies that have been employed, from limitations of the shallow ice approximation in the near summit region, from the assumption of an isotropic flow law [*Mangeney et al.*, 1997], or from the simplicity of the climate forcing. On the other hand, a close match was achieved to the inferred GISPII borehole age profile. Future improvements should arise with attention to the representation of firn densification and inclusion of longitudinal stresses in the flow dynamics and with the use of higher-quality data sets for present-day Greenland surface and basal topography.

[75] Our analyses have also demonstrated the utility of semi-Lagrangian tracer methods for tracking ice age, δ^{18}O, and ice source elevation. GRIP ice has been shown to not necessarily originate from the contemporaneous summit, even far down the core. Especially during periods of strong deglaciation such as near the time of minimal Eemian extent, ice is sourced much more locally than from the contemporaneous summit. This has a significant impact on Eemian climate inferences from the GRIP δ^{18}O record.

[76] Tracing δ^{18}O for different δ^{18}O forcing chronologies has made it clear that for isotropic flow laws, summit migration does not contribute to the strong variability of the Eemian segment of the GRIP δ^{18}O record. This fits logically with the afore mentioned local sourcing of GRIP ice during the Eemian. The sensitivity of downstream δ^{18}O vertical profiles to the ice flow history combined with the quality of signal preservation with high-resolution SL tracing offers the possibility of strong constraints on modeled ice sheet evolution from far from summit ice cores.

[77] Our analyses suggest that conservative bounds on the maximum Greenland Eemian sea level contribution are in the range of 2 m to 5.2 m. Given the complexities of near coastal and near ice margin climate and the fact that ice sheet extent is largely governed by the climate of these regions, we wish to emphasize that the use of a single climate proxy from the summit region for driving interglacial cycles of Greenland ice sheet models is likely the most significant uncertainty in the model-based constraint upon the volume of the Greenland ice sheet during the Eemian period. Attempts to constrain the Eemian excess sea level contribution from Greenland employing model-based analyses such as our own must therefore be indulged in with caution, accepting the reality of the significant sources of error that we have described herein. Significant improvements to bounds on the Greenland sea level contribution during the Eemian interglacial might be achievable with high-resolution tracer analyses for Dye 3 and Camp Century ice cores in combination with a more complete ice sheet model (i.e., that includes firn densification, longitudinal stresses, and more accurate basal and surface elevation data sets). Independent Eemian climate constraints for near margin regions would also be valuable in this context.

[78] A primary reason for attempting to bound the Greenland contribution to the Eemian highstand of sea level is to constrain the residual contribution that must be required from the potentially unstable West Antarctic ice sheet. However, asynchronicity adds another complication to this inference of Antarctic Eemian instability [*Cuffey and Marshall*, 2000]. Given the approximately 3 kyr phase lag between initial Antarctic and Greenland warming after LGM [*Sowers and Bender*, 1995] and the 1.5 to 3 kyr

phase lag for a number of millennial-scale warming events [*Blunier and Brook*, 2001], it is unlikely that both ice sheets would have simultaneously reached their minimum Eemian extent. As such, estimates for Antarctic minima based on residual sea level contributions (i.e., after accounting for Greenland) must be interpreted as lower limits. Greenland extent is, furthermore, largely under more direct climate controls impacting on margin ablation. Grounded West Antarctic ice volume is largely governed by sea level, though subject to thermomechanically induced lags [*Ritz et al.*, 2001]. This, together with the complicated response of northern and southern hemispheric climates to orbital forcing, strongly suggests at least some lack of synchronicity. Even a 2 kyr separation in Eemian minima would translate into an extra 0.6 m of possible sea level contribution for the α_c(Eemian) = 0.364 model. A 3 kyr separation would allow more than double that excess. Given the uncertainties in modeling, it is clear that definitive partitioning of the Eemian excess sea level contribution between the plausible northern and southern hemispheric sources will require additional observational constraints. It nevertheless remains conceivable that much if not the majority of the excessive Eemian highstand of sea level was accounted for by Greenland. This conclusion of our analyses is potentially of great importance in relation to the issue of the possibility that Greenland is the most likely source of the approximately 0.6 mm yr^{-1} contribution to the present-day rate of global sea level rise that may be required to fully explain the otherwise missing contribution for the present-day (but century average) rate of global sea level rise [*Peltier*, 2001; *Douglas and Peltier*, 2002].

[79] **Acknowledgments.** This paper is a contribution to the Climate System History and Dynamics Collaborative Research Network that is funded by the Natural Sciences and Engineering Research Council of Canada and the Atmospheric Environment Service of Canada. Additional support for the work has been provided by NSERC grant A9627. GRIP and GISP II Data were provided by the National Snow and Ice Data Center, University of Colorado at Boulder, and the WDC-A for Paleoclimatology, National Geophysical Data Center, Boulder, Colorado. We would also like to thank Kurt Cuffey for his challenging expresso-fuelled review.

References

Bamber, J. L., R. J. Hardy, P. Huybrechts, and I. Joughin, A comparison of balance velocities, measured velocities and thermomechanically modelled velocities for the Greenland Ice Sheet, *Ann. Glaciol.*, *30*, 211–216, 2000.

Bennike, O., and H. F. Jepsen, A new interglacial sequence from Washington Land, northern Greenland, *Polar Res.*, *9*, 267–270, 2000.

Bermejo, R., On the equivalence of semi-Lagrangian and particle-in-cel finite-element methods, *Mon. Weather Rev.*, *118*, 979–987, 1990.

Bermejo, R., and A. Stanforth, The conversion of semi-Lagrangian advection schemes to quasi-monotone schemes, *Mon. Weather Rev.*, *120*, 2622–2632, 1992.

Blunier, T., and E. J. Brook, Timing of millennial-scale climate change in Antarctica and Greenland during the last glacial period, *Science*, *291*, 109–112, 2001.

Braithwaite, R. J., Positive degree-day factors for ablation on the Greenland ice sheet studied by energy-balance modeling, *J. Glaciol.*, *41*, 153–160, 1995.

Chappellaz, J., T. Blunier, and B. Malize, CH_4 and ^{1}8O of O_2 records from Antarctic and Greenland ice: A clue for stratigraphic disturbance in the bottom part of the Greenland Ice Core Project and Greenland Ice Sheet Project 2 ice cores, *J. Geophys. Res.*, *102*, 26,547–26,557, 1997.

Cheney, W., and D. Kincaid, *Numerical Mathematics and Computing*, 2nd ed., Brooks/Cole, Pacific Grove, Calif., 1985.

Cuffey, K. M., Methodology for use of isotopic climate forcings in ice sheet models, *Geophys. Res. Lett.*, *27*, 3065–3068, 2000.

Cuffey, K. M., and G. D. Clow, Temperature, accumulation and ice sheet elevation in central Greenland through the last deglacial transition, *J. Geophys. Res.*, *102*, 26,383–26,396, 1997.

Cuffey, K. M., and S. J. Marshall, Substantial contribution to sea-level rise during the last interglacial from the Greenland ice sheet, *Nature*, *404*, 591–594, 2000.

Cuffey, K. M., G. D. Clow, R. B. Alley, M. Stuiver, E. D. Waddington, and R. W. Saltus, Large Arctic temperature change at the Wisconsin-Holocene glacial transition, *Science*, *270*, 455–458, 1995.

Dahl-Jensen, D., and N. S. Gundestrup, Constitutive properties of ice at Dye 3, Greenland, the physical basis of ice sheet modeling, *IAHS Publ.*, *170*, 31–43, 1987.

Dahl-Jensen, D., T. Thorsteinsson, R. Alley, and H. Shoji, Flow properties of the ice from the Greenland Ice Core Project ice core: The reason for folds?, *J. Geophys. Res.*, *102*, 26,831–26,840, 1997.

Dahl-Jensen, D., N. G. K. Mosegaard, G. D. C. S. J. Johnsen, A. W. Hansen, and N. Balling, Past temperatures directly from the Greenland ice sheet, *Science*, *282*, 268–271, 1998.

Douglas, B. C., and W. R. Peltier, The puzzle of global sea-level rise, *Phys. Today*, *55*, 35–40, 2002.

Fawcett, P. J., A. M. Agustsdottir, R. B. Alley, C. A. S. S. Funder, and L. Hansen, The Younger Dryas termination and North Atlantic Deep Water formation: Insights from climate model simulations and Greenland ice cores, *Paleoceanology*, *12*, 23–38, 1997.

Greve, R., M. Weis, and K. Hutter, Palaeoclimatic evolution and present conditions of the Greenland ice sheet in the vicinity of Summit: An approach by large-scale modelling, *Palaeoclim. Data Model.*, *2*, 133–162, 1998.

Hendricks, M. B., D. J. Depaolo, and R. C. Cohen, Space and time variation of δ^{18}O and δD in precipitation: Can paleotemperature be estimated from ice cores, *Global Biogeochem. Cycle*, *14*, 851–861, 2000.

Hillaire-Marcel, C., A. de Vernal, G. Bilodeau, and A. J. Weaver, Absence of deep-water formation in the Labrador Sea during the last interglacial period, *Nature*, *410*, 1073–1077, 2001.

Huybrechts, P., The Antarctic ice sheet during the last glacial-interglaical cycle: A three-dimensional experiment, *Ann. Glaciol.*, *14*, 115–119, 1990.

Huybrechts, P., Formation and disintegration of the Antarctic ice sheet, *Ann. Glaciol.*, *20*, 336–340, 1994.

Huybrechts, P., A. Letreguilly, and N. Reeh, The Greenland ice sheet and greenhouse warming, *Palaeogeogr. Palaeoclimato. Palaeoecol.*, *89*, 399–412, 1991.

Janssens, I., and P. Huybrechts, The treatment of meltwater retention in mass-balance parameterizations of the Greenland ice sheet, *Ann. Glaciol.*, *31*, 2000.

Johnsen, S. J., W. Dansgaard, and J. W. C. White, The origin of Arctic precipitation under present and glacial conditions, *Tellus*, *41*, 452–469, 1989.

Johnsen, S. J., D. Dahl-Jensen, W. Dansgaard, and N. S. Gundestrup, Greenland palaeotemperatures derived from GRIP bore hole temperature and ice core isotope profiles, *Tellus*, *47B*, 624–629, 1995.

Johnsen, S. J., et al., The δ^{18}O record along the Greenland Ice Core Project deep ice core and the problem of possible Eemian climatic instability, *J. Geophys. Res.*, *102*, 26,397–26,410, 1997.

Karabanov, E. B., A. A. Propenko, D. F. Williams, and G. K. Khursevich, Evidence for mid-Eemian cooling in continental climatic record from Lake Baikal, *J. Paleolimnol.*, *23*, 365–371, 2000.

Koerner, R. M., Ice core evidence for extensive melting of the Greenland ice sheet in the last interglacial, *Science*, *244*, 964–967, 1989.

Krinner, G., C. Genthon, and J. Jouzel, GCM analysis of local influences on ice core delta signals, *Geophys. Res. Lett.*, *24*, 2825–2828, 1997.

Legates, D. R., and C. J. Willmott, Mean seasonal and spatial variability in gauge-corrected global precipitation, *Int. J. Climatol.*, *10*, 111–127, 1990.

Mangeney, A., F. Califano, and K. Hutter, A numerical study of anisotropic, low Reynolds number, free surface flow for ice sheet modeling, *J. Geophys. Res.*, *102*, 22,749–22,764, 1997.

Marshall, S. J., and K. M. Cuffey, Peregrinations of the Greenland ice sheet divide in the last glacial cycle: Implications for central Greenland ice cores, *Earth Planet. Sci. Lett.*, *179*, 73–90, 2000.

McCalpin, J. D., A quantitative analysis of the dissipation inherent in semi-Lagrangian advection, *Mon. Weather Rev.*, *116*, 2330–2336, 1988.

McDonald, A., Accuracy of mulitply-upstream, semi-Lagrangian advective schemes, *Mon. Weather Rev.*, *112*, 1267–1275, 1984.

Meese, D. A., A. J. Gow, R. B. Alley, G. A. Zielinski, P. M. Grootes, M. Ram, K. C. Taylor, P. A. Mayewski, and J. F. Bolzan, The Greenland Ice Sheet Project 2 depth-age scale: Methods and results, *J. Geophys. Res.*, *102*, 26,411–26,423, 1997.

Ohmura, A., New temperature distribution maps for Greenland, *Z Gletscherkd. Glazialgeol.*, *23*, 1–45, 1987.

[5] A further important question that we will investigate concerns the variability of interglacial climates. The GRIP $\delta^{18}O$ record offers a high-resolution proxy for past climate. Significant high-frequency oscillations appear in the Eemian segment of the ice core. It remains unclear as to the extent to which these oscillations represent actual climate variability or are the result of disturbances to the ice core stratigraphy [*Johnsen et al.*, 1997; *Steffensen et al.*, 1997]. High-frequency climate variability and the associated changes in climatic extremes potentially constitute the most significant impacts of global warming and yet are the most serious challenge to climate change prediction. As such, observations of past climate variability during warmer climate regimes could provide an important complement to model predictions of enhanced variability.

[6] However, the reconstruction of past climates based upon ice core derived profiles of isotopic and chemical tracers requires deconvolution of the stratigraphy of the ice core. If the regional summit of an ice sheet were not horizontally displaced during a glacial cycle and no significant anisotropic effects (folds) were active in the local ice flow, then extraction of an appropriate chronology of climate change from a summit ice core would be much more straightforward. However, it is unlikely that summit location remains stationary and thus the stratigraphic record from an ice core is inevitably disturbed by the flow of upstream ice from adjacent locations and also by the development of folds due to the complexity of ice flow near the bed. The strong correlation between GRIP and GISP II $\delta^{18}O$ profiles for the post-Eemian segment of these ice cores indicates that the stratigraphy of these segments is basically undisturbed. However, the discrepancy between the proximal GRIP and GISP II $\delta^{18}O$ profiles corresponding to the Eemian period makes it clear that one or both of the ice cores have experienced significant stratigraphic deformation from some combination of ice flow and folding effects.

[7] In terms of their present-day geometries, internal temperature fields, internal distributions of isotopes and other tracers, and in the relative sea level histories that are observed in the proximate coastal regions, ice sheets contain a large though convoluted record of their own evolution and the past surface climate and basal thermal inputs that have governed it. Ice sheet models combined with climate models or proxy record-based climate forcings are a powerful tool for deconvolving the climate record that has been subtly recorded in existing ice sheets. One-dimensional (vertical only) thermal models, for example, have been successfully employed in the context of Monte Carlo inversions to extract the Holocene temperature history from the borehole temperature profile at GRIP [*Dahl-Jensen et al.*, 1998]. Three-dimensional thermomechanically coupled ice sheet models offer the potential of a much more complete and self-consistent deconvolution of ice sheet observations to infer variable climate forcing. However, computational costs limit the range of parameter space that they may be employed to probe. Imposition of observational constraints must generally rely on hand tuning, and therefore 3-D model inferences of past climate variability are subject to the uncertainty that exists concerning the uniqueness of the tuning procedure on the basis of which model parameters are fixed.

[8] Here, through the computation of a very large number of solutions of the forward problem, we attempt to significantly raise the bar on the range of constraints that may be imposed on the evolution of a 3-D model of the Greenland ice sheet in order to better constrain its Eemian evolution. These constraints include the following: (1) the observed borehole temperature and age profile at GRIP, (2) basal temperatures at Camp Century and Dye 3, (3) radiocarbon dated relative sea level (RSL) histories from 16 sites distributed quasi-uniformly around the entire coastline of the Greenland subcontinent, and (4) the present-day surface topography (our best models to be discussed in the text that follows deliver an RMS difference of 70 m with respect to the observationally based digital input topography) [*Tarasov and Peltier*, 2002]. The relative sea level, surface topography and age and temperature profile observations impose strong spatial and temporal constraints on ice sheet evolution, as we will demonstrate in the analyses to be reported herein. This is in contrast to previous 3-D modeling analyses that have been limited to area, volume, and a handful of single point constraints (e.g., observed basal temperatures from boreholes), the most extensive study being that of *Greve et al.* [1998]. We will furthermore develop and apply a very high resolution semi-Lagrangian (SL) tracer technique to track ice source elevation and ice age. SL tracer techniques have become preeminent in the numerical weather prediction field but to this point have not been employed for the purpose of glaciological analyses. As a possible further constraint on Eemian ice sheet evolution, we will also use the SL technique to investigate the sensitivity of a model $\delta^{18}O$ tracer field to summit migration and to the isotopic sensitivity to temperature assumed in the model.

[9] Following a brief description of the ice sheet, bedrock, and mass balance models that comprise the three dimensional thermomechanically coupled model of ice sheet evolution that is employed for this study, and of the applied climate forcing, we will present in what follows a detailed description and intercomparison of a suite of semi-Lagrangian (SL) tracer modules, that may be employed to track ice age, $\delta^{18}O$, and ice source elevation. We will then investigate the extent to which observed basal temperatures from boreholes in the ice sheet can be used to invert the poorly constrained deep geothermal heat flux. An examination of the sensitivity of the predicted borehole temperature profile to the assumed paleothermometric calibration brings clearly to the fore the complexity involved in tuning a model of this kind to infer the "correct" paleothermometric calibration. Model predicted borehole temperatures and age profiles for the GISP II and NGRIP sites will also be discussed. Using a $\delta^{18}O$ model tracer field that clearly resolves major Eemian fluctuations, we examine the role of flow disturbances arising from movement of the contemporaneous summit on the apparent $\delta^{18}O$ chronology inferred from GRIP. Finally, taking into account ice source elevation in the climate inversion from the $\delta^{18}O$ record, we obtain new bounds on the possible Greenland contribution to excess Eemian sea level. Modeled ice source elevation and age profiles for NGRIP are also discussed.

2. Discussion of Model Components

[10] The 3-D ice sheet model (ISM) that we have developed and employ herein has full thermomechanical cou-

Ohmura, A., and N. Reeh, New precipitation and accumulation maps for Greenland, *J. Glaciol.*, *37*, 140–148, 1991.

Ohmura, A., P. Calanca, M. Wild, and M. Anklin, Precipitation, accumulation and mass balance of the Greenland ice sheet, *Z. Gletscherkd. Glazialgeol.*, *35*, 1–20, 1991.

Oppo, D. W., L. D. Keigwin, J. F. McManus, and J. L. Cullen, Persistent suborbital climate variability in marine isotope stage 5 and termination II, *Paleoceanography*, *16*, 280–292, 2001.

Peltier, W. R., The impulse response of a Maxwell Earth, *Rev. Geophys.*, *12*, 649–669, 1974.

Peltier, W. R., Glacial isostatic adjustment ii: The inverse problem, *Geophys. J. R. Astron. Soc.*, *46*, 669–706, 1976.

Peltier, W. R., Mantle viscosity and ice age ice sheet topography, *Science*, *273*, 1359–1364, 1996.

Peltier, W. R., Postglacial variations in the level of the sea: Implications for climate dynamics and solid-earth geophysics, *Rev. Geophys.*, *36*, 603–689, 1998.

Peltier, W. R., Global glacial isostatic adjustment and modern instrumental records of relative sea level history, in *Sea Level Rise: History and Consequences*, edited by B. C. Douglas, M. S. Kearney, and S. P. Leatherman, pp. 65–95, Academic, San Diego, Calif., 2001.

Peltier, W. R., and X. Jiang, Mantle viscosity from the simultaneous inversion of multiple data sets pertaining to postglacial rebound, *Geophys. Res. Lett.*, *23*, 503–506, 1996.

Pollack, H. N., S. J. Hurter, and J. R. Johnson, Heat flow from the Earth's interior: Analysis of the global data set, *Rev. Geophys.*, *31*, 267–280, 1993.

Raymond, C. F., Deformation in the vicinity of ice divides, *J. Glaciol.*, *29*, 357–373, 1983.

Raynaud, D., J. Chappellaz, C. Ritz, and P. Martinerie, Air content along the Greenland Ice Core Project core: A record of surface climatic parameters and elevation in central Greenland, *J. Geophys. Res.*, *102*, 26,607–26,613, 1997.

Reames, F. M., and T. H. Zapotocny, Inert trace constituent transport in sigma and hybrid isentropic-sigma models, part ii, Twelve semi-Lagrangian algorithms,, *Mon. Weather Rev.*, *127*, 188–200, 1999.

Ritz, C., A. Fabre, and A. Letreguilly, Sensitivity of a Greenland ice sheet model to ice flow and ablation parameters: Consequences for evolution through the last climatic cycle, *Clim. Dyn.*, *13*, 11–24, 1997.

Ritz, C., V. Rommelaere, and C. Dumas, Modeling the evolution of Antarctic ice sheet over the last 420,000 years: Implications for altitude changes in the Vostok region, *J. Geophys. Res.*, *106*, 31,943–31,964, 2001.

Rostami, A., W. R. Peltier, and A. Mangini, Quaternary marine terraces, sea level changes and uplift histoyr of Patagonia, Argentian: Comparisons with predictions of the ICE-4G (VM2) model of the global process of glacial isostatic adjustment, *Quat. Sci. Rev.*, *19*, 1495–1525, 2000.

Sass, J. H., B. L. Nielsen, H. A. Wollenberg, and R. J. Munroe, Heat flow and surface radioactivity at two sites in South Greenland, *J. Geophys. Res.*, *77*, 6435–6444, 1972.

Schott-Hvidberg, C., D. Dahl-Jensen, E. D. Waddington, and J. F. Bolzan, Ice flow between the Greenland Ice Core Project and Greenland Ice Sheet Project 2 boreholes in central Greenland, *J. Geophys. Res.*, *102*, 26,851–26,859, 1997.

Shuman, C. A., R. B. Alley, S. Anandakrishnan, J. W. C. White, P. M. Grootes, and C. R. Stearns, Temperature and accumulation at the Greenland Summit: Comparison of high-resolution isotope profiles and satellite passive microwave brightness temperature trends, *J. Geophys. Res.*, *100*, 9165–9177, 1995.

Shuman, C. A., R. B. Alley, M. A. Fahnestock, R. A. Bindschadler, J. W. C. White, J. Winterle, and L. R. McConnell, Temperature history and accumulation timing for the snowpack at GISP2, central Greenland, *J. Glaciol.*, *146*, 21–30, 1998.

Sowers, T., and M. Bender, Climate records covering the last deglaciation, *Science*, *269*, 210–214, 1995.

Staniforth, A., and J. Cote, Semi-Lagrangian integration schemes for atmospheric models—A review, *Mon. Weather Rev.*, *119*, 2206–2223, 1991.

Steffensen, J. P., H. Clausen, C. U. Hammer, M. Legrand, and M. DeAngelis, The chemical composition of cold events within the Eemian section of the Greenland Ice Core Project ice core from Summit Greenland, *J. Geophys. Res.*, *102*, 26,747–26,754, 1997.

Tarasov, L., and W. R. Peltier, Impact of thermomechanical ice sheet coupling on a model of the 100 kyr ice age cycle, *J. Geophys. Res.*, *104*, 9517–9545, 1999.

Tarasov, L., and W. R. Peltier, Greenland glacial history and local geodynamic consequences, *Geophys. J. Int.*, *150*, 198–229, 2002.

Vezina, J., B. Jones, and D. Ford, Sea-level highstands over the last 500,000 years: Evidence from the Ironshore formation on Grand Cayman British West Indies, *J. Sediment. Res.*, *69*, 317–327, 1999.

Werner, M., U. Mikolajewicz, M. Himann, and G. Hoffmann, Borehole versus isotope temperatures on Greenland: Seasonality does matter, *Geophys. Res. Lett.*, *27*, 723–726, 2000.

White, J. W. C., L. K. Barlow, D. Fisher, P. Grootes, J. Jouzel, S. J. Johnsen, M. Stuiver, and H. Clausen, The climate signal in the stable isotopes of Summit, Greenland: Results of comparisons with modern climate observations, *J. Geophys. Res.*, *102*, 26,425–26,439, 1997.

Williamson, D. L., and P. Rasch, Two-dimensional semi-Lagrangian transport with shape-preserving interpolation, *Mon. Weather Rev.*, *117*, 102–129, 1989.

World Data Center-A for Paleoclimatology, National Geophysical Data Center, The Greenland Summit Ice Cores [CD-ROM], Boulder, Colo., 1997. (Available at http://www.ngdc.noaa.gov/paleo/icecore/greenland/summit/).

W. R. Peltier and L. Tarasov, Department of Physics, University of Toronto, Toronto, Ontario, Canada M5S 1A7. (peltier@atmosp.physics.utoronto.ca; lev@atmosp.physics.utoronto.ca)

Table 1. Model Parameters

Definition	Parameter	Value
Earth radius	R_E	6370 km
Earth mass	m_e	5.976×10^{24} kg
Lithospheric thickness	L_e	100 km
Latent heat of fusion	L	3.35×10^5 J kg^{-1}
Ice density	ρ_i	910 kg m^{-3}
Ice specific heat capacity	$c_i(T)$	(152.5 + 7.122T) J kg^{-1} K^{-1}
Ice thermal conductivity	$k_i(T)$	9.828 exp(−0.0057T) W m^{-1} K^{-1}
Bedrock density	ρ_b	3300 kg m^{-3}
Bedrock specific heat capacity	c_b	1000 J kg^{-1} °C^{-1}
Bedrock thermal conductivity	k_b	3 W m^{-1} °C^{-1}
Standard deviation, PDD model	σ	5.2 °C
Standard deviation, accumulation model	σ_p	σ − 1 °C
Exponential factor, precipitation rate	η	0.062 °C^{-1}
Number of ice thermodynamic levels	nz_i	65
Number of bed thermodynamic levels	nz_b	5
Longitudinal ISM grid resolution	$\Delta\phi$	0.5°
Latitudinal ISM grid resolution	$\Delta\theta$	0.25°
Weertman sliding law rate factor	k_s	1.8×10^{-10} Pa^{-3} m2 yr^{-1}
Glen flow law constant, T < −10°C	B_{gc}	1.14×10^{-5} Pa^3 yr^{-1}
Glen flow law constant, T > −10°C	B_{gw}	5.47×10^{10} Pa^3 yr^{-1}
Flow law enhancement factor for glacial ice	E	5.1
Flow law enhancement factor for Holocene ice	E_h	E/2.5
Creep activation energy of ice, $T < -10$°C	Q_c	6×10^4 J mol^{-1}
Creep activation energy of ice,T > −10°C	Q_c	1.39×10^5 J mol^{-1}
Glen flow law exponent	n	3
Glacial δ^{18}O sensitivity to temperature	α_{cG}	0.312 (GrB), 0.33(GrC)
Holocene δ^{18}O sensitivity to temperature	α_c(Holocene)	0.364 (GrB), 0.25 (GrC)
Late Holocene δ^{18}O sensitivity	α_{cLH}	0.6 (GrB),0.47 (GrC)

pling (including bed thermodynamics). It is coupled asynchronously to a physically based viscoelastic model of the glacial isostatic adjustment process to describe the time-dependent displacement of the surface of the solid earth due to surface loading and to a positive degree-day surface mass balance model with temperature-dependent degree-day coefficients and physically based refreezing model. Model parameters that appear in the discussion to follow are summarized in Table 1.

2.1. Thermomechanical Ice Sheet and Bedrock Response Models

[11] The base thermomechanically coupled model is that originally described by *Tarasov and Peltier* [1999] with more recent improvements and Greenland specific details provided by *Tarasov and Peltier* [2002]. Only a brief review of these primary components will be provided here. The ice dynamics component of the model is based upon the vertically integrated form of the equation for the conservation of mass, as

$$\frac{\partial H}{\partial t} = -\nabla_h \cdot \int_{z_b}^{h} \mathbf{V}(z)dz + G(\mathbf{r}, T), \quad (1)$$

in which H is local ice thickness and G is the net surface and basal mass balance. The standard Glen flow law for ice rheology is employed to compute the horizontal ice velocity $\mathbf{V}(z)$ with a factor 5.1 flow enhancement (unless otherwise stated). The temperature dependence of the ice rheology is as per the European Ice Sheet Modeling Initiative (EISMINT) II intercomparison project specifications (available at http://gopher.ulb.ac.be/phuybrec/eismint.html; also see C. Ritz et al., manuscript in preparation, 2002). A factor 2.5 reduction of the flow parameter is applied to interglacial ice (i.e., ice that formed during either the Holocene or Eemian periods) in accord with observations [*Dahl-Jensen and Gundestrup*, 1987].

[12] The computation of the ice temperature field (T) is based on the conservation of internal energy and takes into account advection, vertical diffusion, and heat generated by deformation heating (Q_d) as represented by the following partial differential equation:

$$\rho_i c_i(T)\frac{\partial T}{\partial t} = \frac{\partial}{\partial z}\left\{k_i(T)\frac{dT}{dz}\right\} - \rho_i c_i(T)\mathbf{V}\cdot\nabla T + Q_d. \quad (2)$$

Heating due to sliding is accounted for in the basal thermal boundary conditions as discussed by *Tarasov and Peltier* [1999]. The thermodynamic solver is fully coupled to the ice dynamics module, and in the base configuration includes 65 levels in the vertical scaled to the local ice thickness. The model for the internal temperature field is also implicitly coupled to a 5 level thermodynamic (vertical diffusion of heat only) bedrock model that spans a depth of 2 km. The deep geothermal heat flux employed herein as the lower boundary condition for the thermodynamic bedrock model is described in a subsequent section.

[13] Bedrock response is computed on the basis of a complete linear viscoelastic field theory for a spherically symmetric Maxwell model of the Earth [*Peltier*, 1974, 1976]. For an arbitrary surface load per unit area $L(\theta, \Psi, t)$, the bedrock displacement $R(\theta, \psi, t)$ is governed by the following space-time convolution:

$$R(\theta,\psi,t) = \int_{-\infty}^{t}\int\int_{\Omega} L(\theta',\psi',t')\Gamma(\gamma,t-t')d\Omega' dt', \quad (3)$$

in which $\Gamma(\gamma, t - t')$ is the radial displacement Green function [*Peltier*, 1974]. The radial response is evaluated using a spectral representation [*Peltier*, 1976] of the convolution integral (3) truncated at degree and order 256.The radial viscosity profile is represented by that of the VM2 model [*Peltier*, 1996; *Peltier and Jiang*, 1996] with a 90 km thick lithosphere and the PREM model [*Dziewonski and Anderson*, 1981] is assumed to describe the elastic structure. Bedrock response is computed every 100 years and is asynchronously coupled to the ice sheet model. The model is initialized with the present-day observed surface and bedrock topography. It is first brought to thermomechanical equilibrium (under the assumption of isostatic equilibrium) using the climate forcing inferred for 250 ka. The model is then run with full dynamical coupling from 250 ka to present using a climate forcing based primarily upon the summit $\delta^{18}O$ record as discussed below. A more complete description of the isostatic adjustment model is provided by *Tarasov and Peltier* [2002] while the relative sea level solver has been reviewed by *Peltier* [1998].

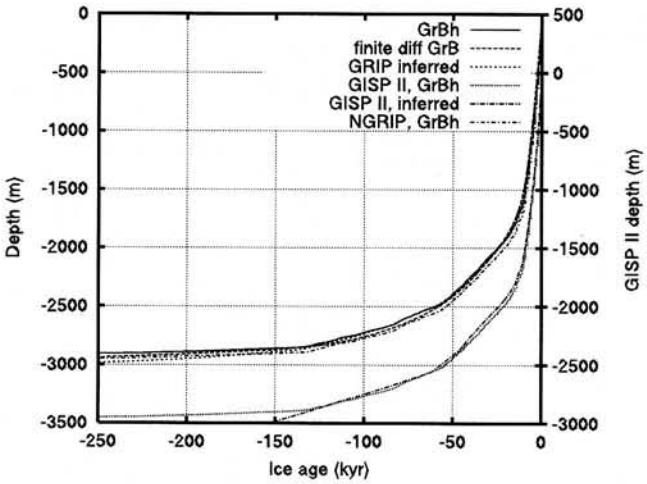

Figure 1. Age profiles at GRIP, GISP II, and NGRIP computed with tricubic spline tracer. Also shown for comparison is the age profile for GRIP computed with a finite difference tracer module.

2.2. Mass Balance Model

[14] The surface mass balance model is based upon a positive degree-day representation of the ablation process with temperature-dependent positive degree-day coefficients derived from the analyses of *Braithwaite* [1995]. The influence of surface refreezing is included, taking into account both capillary retention and latent heating following the methodology of *Janssens and Huybrechts* [2000].

[15] As has become standard for ice sheet models that are not explicitly coupled to General Circulation Models of climate evolution, precipitation is computed by assuming a surface temperature-dependent perturbation to the present-day observed precipitation climatology $P(0, x, y)$, as follows:

$$P(t,x,y) = P(0,x,y)\gamma \; exp\Big[\eta \; \eta_{xy}(x,y)\Delta T(t,x,y)\Big], \qquad (4)$$

with a base value of 0.062 for the parameter η, chosen to provide a good fit to both the inferred age profile of the GRIP ice core (see Figure 1) and to the observed borehole temperature profile.

[16] We have also found it necessary to explicitly allow for some regional sensitivity of the local precipitation rate upon temperature (represented by the parameter $\eta_{xy}(x, y)$ in equation (4)) in order to better fit relative sea level observations from the coast of Greenland as well as additional topographic constraints. Briefly, $\eta_{xy}(x, y)$ is linearly reduced to 0.5 from 68°N to 60°N (then held at 2.0 south of 60°N), is increased to 2.0 in the northeastern sector of the ice sheet and is elsewhere equal to 1.0. The southern zone reduction in $\eta_{xy}(x, y)$ offsets the decrease in glacial precipitation due to the stronger climate forcing imposed in that region as described in section 2.3.

[17] A slope-dependent factor γ is also included to capture orographic impacts on precipitation and follows the form employed by *Ritz et al.* [1997] though with an added weakening of the slope-dependence with elevation so as to better match observed borehole temperature and age profiles and inferred accumulation rate history at GRIP. Specifically, γ is defined as

$$\gamma = \left(1 - \frac{h}{4\ \text{km}}\right) \min\left[1.5,\ \frac{||\nabla h(x,y,t)|| + 0.001}{||\nabla h(\text{observed})|| + 0.001}\right] + \frac{h}{4\ \text{km}}, \qquad (5)$$

where h is the surface elevation. The resulting accumulation rate history that is predicted by the model for the GRIP site, shown in Figure 2, is at almost all ages less than that inferred for GRIP by *Johnsen et al.* [1995] but generally lies above that inferred for the nearby GISP II site by *Cuffey and Clow* [1997]. The age profile for our base model (denoted GrB) at both the GRIP and GISP II sites, as shown in Figure 1, matches the corresponding inferred age profiles to within the well-constrained GISP II age profile uncertainties discussed by *Meese et al.* [1997], at least for the top 2860 m (corresponding to approximately the last 150 kyr). At the GRIP site, a 60 m model misfit in ice thickness results in discrepancies for the bottom of the core.

[18] The present-day precipitation climatology utilized in the model was presented by *Tarasov and Peltier* [2002] and is a combination of results obtained from the inversion of a new digital accumulation map for higher elevations [*Ohmura et al.*, 1991] and an older precipitation map for lower elevations [*Ohmura and Reeh*, 1991] with present-day seasonal variability taken from *Legates and Willmott* [1990]. Snow fraction is computed assuming a normal distribution for temperatures around monthly means with solid fraction assumed for temperatures below 2°C.

[19] Calving of ice is a key component of Greenland mass balance. The representation of calving processes is problematic in light of the subgrid-scale processes involved. Given the lack of a consensus alternative, we simply calve ice in proportion to the excess buoyancy of the marginal ice with the time-independent proportionality factor hand-tuned to provide a match between model and observed relative sea

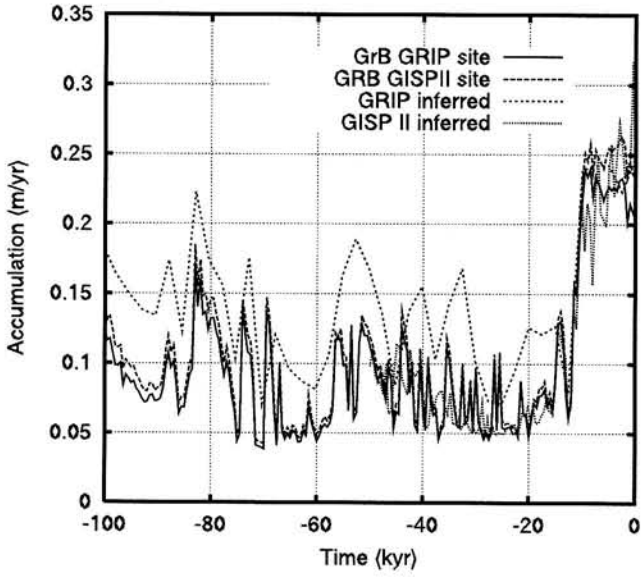

Figure 2. Accumulation chronology at GRIP and GISP II. Inferred GRIP chronology is from *Johnsen et al.* [1995]. Inferred GISPII chronology is from *Cuffey and Clow* [1997].

level chronologies as detailed by *Tarasov and Peltier* [2002].

2.3. Temperature Forcing: Determination of the Proxy for Climate Variability

[20] We use the δ^{18}O GRIP record as a proxy for regional climate variations and constrain the climatic isotopic sensitivity $\alpha_c = d\delta^{18}\mathrm{O}/\mathrm{dT}$ to be less than the present-day spatial sensitivity of approximately 0.67‰ $^{\circ}\mathrm{C}^{-1}$. Holocene and glacial values for α_c are obtained so as to provide a close match between the model and observed borehole temperature profile at GRIP. Following *Cuffey* [2000], we will take into account the effect of the observed isotopic lapse rate in central Greenland on the temporal transfer function from δ^{18}O to temperature forcing. Specifically, using the observed value for the δ^{18}O lapse rate in central Greenland of $\lambda_\delta = -6.2‰\ \mathrm{km}^{-1}$ [*Johnsen et al.*, 1989], the regional climate forcing ΔT_c will be assumed to be given by

$$\Delta T_c(t) = \frac{\Delta\delta^{18}\mathrm{O}(t) - [\lambda_\delta \Delta Z_G(t)])}{\alpha_c(t)}, \tag{6}$$

in which $\Delta Z_G(t)$ is the change in surface elevation relative to present-day at the GRIP site. Surface temperature change is then computed from ΔT_c using a constant environmental lapse rate of 7.5°C km^{-1}. Present and past surface temperature gradients are computed with the widely used parameterization of *Huybrechts et al.* [1991] based on the surface temperature maps of *Ohmura* [1987].

[21] The largest single uncertainty in glacial cycle modeling of large-scale ice sheets is that of the accuracy of the climate forcing. Given the variability of midlatitude storm tracks and their impact on regional Greenland climate, especially during glacial periods, the use of a single proxy to drive climate changes over all of Greenland is clearly suspect. Using constraints from RSL observations [*Tarasov and Peltier*, 2002] and observed borehole temperature profiles, we have found it necessary to include three further modifications to the regional temperature forcing. First, we have imposed at 5% per degree latitude increase in the amplitude of the δ^{18}O derived temperature forcing (relative to present-day) for all areas south of summit. This is in approximate accord with the results of paleothermometry for the Dye 3 borehole which indicates a 50% larger amplitude in the temperature signal there [*Dahl-Jensen et al.*, 1998], which is most probably due to the closer proximity to the North Atlantic storm track which is thought to have migrated northward during glacial periods [e.g., *Fawcett et al.*, 1997]. Second, we have imposed a set of ad hoc regional modifications to the Holocene temperature forcing in order to obtain a close match with observed relative sea level (RSL) histories and present-day net mass balance estimates for the whole ice sheet [*Tarasov and Peltier*, 2002]. These further modifications are applied only to the near marginal regions(ablation zone) and therefore have no direct thermal impact on the borehole temperature profile for the summit region ice cores. Third, we have also added a slight 0.3°C warming and cooling during the last 1.2 kyr in order to obtain a better match to the observed borehole temperature profile. In detail, the temperature forcing is lowered by −0.3°C linearly from 1.2 ka to 900 years before present and then elevated linearly to the unmodified level by the present time.

2.4. Semi-Lagrangian Tracer Module

[22] Passive tracer fields (F) such as ice formation date and δ^{18}O ratios for ice parcels are conservatively advected through the ice. Their transport is therefore described by

$$\frac{\partial F}{\partial t} = -\mathbf{V} \cdot \nabla F \tag{7}$$

with appropriate boundary conditions at the external surfaces of the ice sheet.

[23] *Tarasov and Peltier* [2002] described the implementation of a finite difference tracer module for transporting the ice parcel formation date through the ice. Application of this module to track δ^{18}O ratios was found to be problematic due to the action of excessive dissipation. Dissipation can be reduced through the use of higher-order finite difference methods and increased resolution, but only at great computational cost. Numerical representations of advective transport using finite difference methods are subject to the CFL criterion that constrains advective transport to advance no more than a single grid cell per computational time step. The semi-Lagrangian methodology avoids this limit and easily extends to higher-order form. Semi-Lagrangian methods assign transported field values based on the value of the field at the precursor point from the previous time step [e.g., *Staniforth and Cote*, 1991]. This is the point $(\mathbf{x} - \mathbf{U}^*\delta t)$ from which the contemporaneous velocity field $\mathbf{U}^*$ would have transported the tracer field $F(t, \mathbf{x})$ to the current grid point over one tracer time step, i.e.,

$$F(t, \mathbf{x}) = F(t - \delta t, \mathbf{x} - \mathbf{U}^*\delta t). \tag{8}$$

[24] Application of this methodology requires two computations every tracer time step. First, an appropriate mean velocity field $\mathbf{U}^*$ must be computed so that a precursor point

can be determined. Second, the value of the field at the precursor point (which is generally not a grid point) must be computed using some form of interpolation. Previous theoretical and analytical studies have generally found that while at least a third-order interpolation scheme is required for the interpolation of the field value to the precursor point, linear interpolation is adequate for determining the midpoint velocity value that is used to represent an effective mean time step velocity [*Staniforth and Cote*, 1991].

[25] The midpoint mean velocity **U*** is obtained from the condition

$$0.5[\mathbf{U}(t, \mathbf{x} - \mathbf{U}^* \cdot \delta t/2) + \mathbf{U}(t - \delta t, \mathbf{x} - \mathbf{U}^* \cdot \delta t/2)] = \mathbf{U}^* \quad (9)$$

and could be interpreted as implementation of the midpoint form of numerical integration. As a test of the stability of the method, we have also implemented an alternative expression for the midpoint field that corresponds to the trapezoidal form of numerical integration, namely:

$$\mathbf{U}^* = 0.5[\mathbf{U}(t - \delta t, \mathbf{x} - \mathbf{U}^* \cdot \delta t) + \mathbf{U}(t, \mathbf{x})]. \quad (10)$$

Use of this form for **U*** resulted in no discernible difference for a sine wave test field as compared to the prior **U*** form. The above recursive equation for **U*** is iterated up to a maximum of 5 times or until the weighted point-wise difference in computed midpoint position between iterations is <3 m. The explicit mathematical form of this condition is then

$$|x_n - x_{n-1}| + |y_n - y_{n-1}| + 10^3|z_n - z_{n-1}| < 3 \text{ m}. \quad (11)$$

For each tracer time step, the previous **U*** field is used to initiate the iterations.

[26] Field values for precursor points situated above the ice sheet surface are set to the contemporaneous surface value of $\delta^{18}O(T_{surface}, h)$, as inverted on the basis of the temperature forcing (determined by equation (6)), and zero age (or, numerically, the ice formation date is set to the contemporaneous time). To allow finer resolution, the tracer module is implemented on a subgrid that does not cover the whole ice sheet. The resolution of the subgrid is given in Table 2. Aside from investigations incorporating the NGRIP site, the subgrid was bounded by 40.25° and 34.25° west longitude and by 71.1° and 74.1° north latitude so as to incorporate all contemporaneous summit positions that obtain during the transient run. Experiments with an expanded horizontal subgrid boundary found no discernible impact on near-GRIP site tracer field results.

[27] It should be noted that since an age field is only computed for the subgrid region, the interglacial flow parameter reduction described above is only applied in the region of the subgrid for model runs using the SL tracer module. Model runs without the SL tracer module use a coarse resolution finite difference tracer calculation to compute age fields for the whole ice sheet. Sensitivity analyses (not shown) indicate that this geographic restriction of the flow enhancement has a relatively minor impact on the modeled ice sheet, at least for the analyses presented herein.

[28] We have found tricubic spline interpolation [e.g., *Cheney and Kincaid*, 1985] to be the most accurate given available computational resources. It also has the useful feature of conserving mass for divergence-free flows [*Bermejo*, 1990]. In the tricubic spline case, the interpolation is centered around the point in question. For precursor points near the horizontal boundary of the subgrid, the tracer model reverts to lowest-order bilinear interpolation horizontally but still remains cubic spline for the vertical interpolation. In order to ensure stability, points with ice thickness less than 100 m are assigned surface boundary values throughout the depth.

Table 2. SL Tracer Model Parameters

Definition	Parameter	Value
Time step	Δt_{SL}	500 → 20000 years
Number of subgrid tracer levels	nz_{SL}	1023
Longitudinal SL subgrid resolution	$\Delta\phi_{SL}$	0.05° → 0.03125°
Latitudinal SL subgrid resolution	$\Delta\theta_{SL}$	0.025° → 0.015625°

[29] Three-dimensional interpolation is very intensive numerically and generally involves a Cartesian product of 1-D interpolations that in this case first involves interpolation onto the z plane of the point in question, followed by interpolation within this horizontal plane. For this reason, a fourth-order 3-D interpolation will require a minimum of 64 linear interpolations for each point. In order to preserve the phase and low- to midfrequency amplitude components of the Eemian segment of the tracer $\delta^{18}O$ chronology in the model and remain within available computational resources, we have found the best trade-off between accuracy and resources to be obtained with a 1/32° by 1/64° horizontal (longitude, latitude) resolution and 1025 equidistant layers in the vertical for the tracer subgrid. This vertical resolution corresponds to a temporal resolution at the GRIP site of about 1200 years at 2750 m which corresponds to a time approximately 100 kyr ago. Theoretical analyses indicate that amplitude and phase errors of SL tracer results are affected by both the relative wavelength (wavelength/grid size) and by the Courant number ($u\Delta t/\Delta x$) [*McDonald*, 1984]. Phase error decreases with the Courant number while amplitude errors are minimized for near integer values of the Courant number. For deep ice (corresponding to Eemian or pre-Eemian periods) in the summit region, the Courant number for the coarse resolution ISM grid is less than 0.03 for the horizontal projection. The presence of significant dissipation with tracer models using this coarse horizontal resolution makes it clear that the Courant number is not the critical factor here. Increased relative wavelength will decrease both phase and amplitude errors. Analyses suggest that a relative wavelength of order 10 or greater is generally required to avoid significant dispersion and dissipation over long-term integrations [*McCalpin*, 1988]. This obviously justifies the need for high vertical resolution. Given the significant improvement of the tracer signal with higher horizontal resolution that is clearly evident in Figure 3, it is evident that even the horizontal projection of the $\delta^{18}O$ signal has significant high-frequency variability. This is especially true near the summit, where the very low horizontal ice velocities and diverging flow results in short relative wavelengths.

[30] It is generally observed that dissipation decreases with increasing time step [*McCalpin*, 1988] due to the decrease in the total number of interpolations involved. In

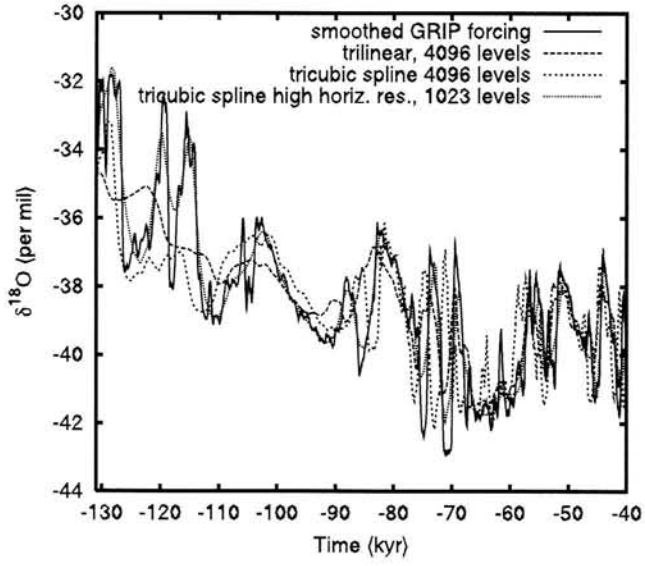

Figure 3. Tracer model comparison for $\delta^{18}O$ chronology at GRIP using a 500 year box smoothed GRIP record for the tracer input with no $\delta^{18}O$ lapse rate effect. Models with 4096 levels use the coarse ISM horizontal resolution.

fact, if the precursor point could be determined exactly, then dissipation and dispersion error would be minimized by using a single time step [*McDonald*, 1984]. There is a trade-off with shorter time steps needed to reduce uncertainty in the precursor point and to maintain temporal resolution of the tracer field near the boundaries. As such, we vary the tracer time step from 500 to 20000 years, with shorter time steps reserved for periods of interest (e.g., the Eemian). Tests with different tracer time steps had no impact on tracer signal phases. Tracer amplitudes for, say, the Eemian segments of model cores were generally improved using large post-Eemian time steps for the tracer module.

2.5. Intercomparison of Different Semi-Lagrangian Tracer Methodologies

[31] An extensive comparison of different semi-Lagrangian (SL) models was undertaken using the ISM horizontal resolution of 0.5 by 0.25 degrees longitude/latitude. Both linear and quadratic interpolations for the midpoint velocity determination were compared, as were linear, cubic spline, and order 3 to 7 Newton-Lagrange interpolation methods (a comparison of a number of these methodologies for a 10 kyr sine wave test forcing is shown in Figure 4). This has led us to the following conclusions that may be valuable to others involved in similar work.

[32] First, even finite difference methods work reasonably well for smooth monotonic fields such as ice age, though discernible improvements are obtained with higher-order SL tracers.

[33] Second, for fields with strong high-frequency variance, such as $\delta^{18}O$, tricubic spline interpolation combined with high horizontal and vertical resolution are required to preserve signal phase and amplitude into the Eemian period as demonstrated in Figure 3. For more recent periods, horizontal resolution can be degraded without significant impact. Trilinear interpolation is not appropriate for signals with high-frequency variance.

[34] Third, in accord with experience in the numerical weather prediction field, higher-order interpolation for the midpoint evaluation did not produce any significant improvements in the quality of the tracer signal recovered.

[35] Fourth, tricubic spline interpolation for the determination of the tracer field value at the precursor point preserves tracer signal quality better than even eighth-order Newton-Lagrange interpolation with quasi-monotonic constraints. Other studies [*Reames and Zapotocny*, 1999] find no significant improvement in tracer field conservation with Newton-Lagrange interpolation using orders higher than 8.

[36] We have also explored the impact of employing quasi-monotonic constraints on the precursor field value interpolation. This constraint enforces the bounding of interpolation results by the extremal values at the grid box vertices enclosing the point in question [*Bermejo and Stanforth*, 1992; *Williamson and Rasch*, 1989]. Newton-Lagrange interpolation requires such a constraint to avoid significant spurious overshoots of the signal. Spline interpolations can also overshoot, but for the $\delta^{18}O$ signal the overshoots were relatively insignificant. Furthermore, for the sine wave test field, the imposition of quasi-monotonic constraints does slightly increase signal dispersion in accord with previous studies [*Bermejo and Stanforth*, 1992].

[37] In summary, the high-resolution tricubic spline method appears to be the most computationally efficient SL tracer methodology to employ with ice sheet models for signals with high-frequency variance. We are able to preserve phase and a significant fraction of amplitude at the GRIP site reaching back to the Eemian interglacial. For the top section of the model core corresponding to the last 60 kyr, we have near complete capture of the $\delta^{18}O$ signal at the computational temporal tracer resolution.

2.6. A Summary of the Characteristics of the Baseline Model of the History of the Greenland Ice Sheet: GrB

[38] As detailed by *Tarasov and Peltier* [2002], our model version GrB is tuned to five primary constraints:

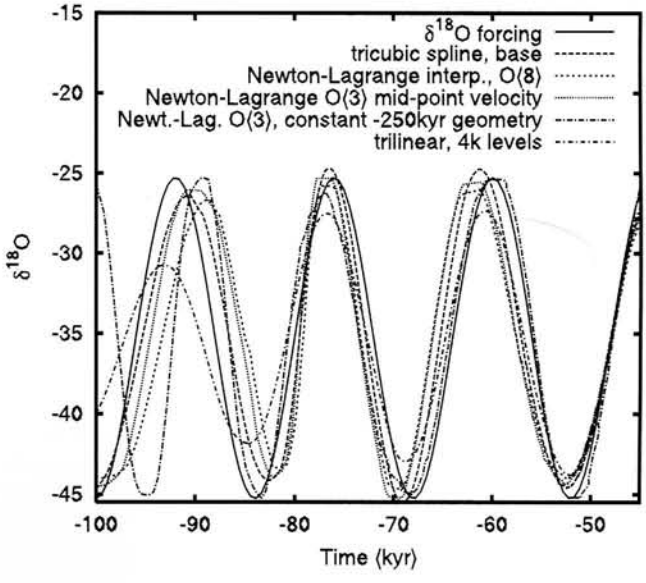

Figure 4. Tracer model comparison for 16 kyr sine wave test field at GRIP site. The different tracer models are discussed in the text.

Table 3. Tuning Parameters

Parameter	Main Effect
Flow enhancement parameter	summit elevation and topographic fit
Sliding parameter	summit elevation and topographic fit
Regional Holocene climate forcing	RSL match
Regional calving sensitivity	RSL match
Precipitation sensitivity	GRIP/GISP inferred accumulation chronology bounds, Age and temperature profile at GRIP
Regional precipitation sensitivity	RSL match and Dye 3 ice thickness
α_c (glacial, Holocene, late Holocene)	GRIP borehole temperature profile
Deep geothermal flux	GRIP borehole temperature profile and Camp Century and Dye 3 basal temperature
Southern climate forcing gradient	Dye 3 ice thickness and basal temperature

surface elevation at summit (GRIP), borehole age, and temperature profiles at GRIP, a set of ^{14}C dated RSL records, and approximate basal temperatures at Camp Century, Dye 3, and GRIP. Secondary constraints that were not necessarily fully compatible with the primary constraints include GRIP accumulation chronology between that inferred for GRIP and GISPII, minimized RMS difference with the observed surface topography, minimized discrepancy with the observed ice volume, and closeness of fit to observed ice thickness at GRIP, Camp Century, and Dye 3. Tuning parameters for these constraints are summarized in Table 3.

[39] With respect to observations, discrepancies in ice thickness (secondary constraint) range from about 65m at GRIP to about 250 m at Dye 3. It is clear from Table 4 that many of these differences are attributable to errors and resolution limitations associated with the input topography, though other factors such as the simplicity of the climate forcing used to drive the model, the assumption of contemporaneous isostatic equilibrium for model initialization at 250 ka, and the lack of explicit ice stream dynamics must also play a role. The overall RMS topographic difference of the ice sheet with respect to the digitized observational topography that was used to initialize the model is a respectable 70 m. Model GrB also has the advantage of a perfect (to grid resolution) match to present-day summit location which provides some minimum confidence in our subsequent analyses of summit migration. Figure 5 shows a sequence of snapshots of the predicted evolutionary history of Greenland, in terms of topography, from the baseline GrB reconstruction developed by *Tarasov and Peltier* [2002]. It is notable that for this model the Eemian configuration of the ice sheet at 121 ka is not significantly different from the present configuration of the ice sheet.

3. Results

3.1. Borehole Temperature Profiles and Geothermal Heat Flux

[40] The deep geothermal heat flux from the Earth into the base of the Greenland ice sheet is largely unknown. The most recent and thorough attempt to develop a global heat flux map is based on a mixture of direct observations and bedrock geology [*Pollack et al.*, 1993]. According to this model, which is illustrated in Figure 6 for the region of Greenland, a strong horizontal gradient should exist across this region. However, the lack of local heat flow measurements in this region leaves the model poorly constrained.

[41] Determination of background geothermal heat flux through the inversion of observed borehole basal temperatures using thermomechanically coupled ice sheet (and bedrock) models offers the possibility of further constraining the geothermal heat flux for ice-covered regions. Direct input of the heat flux map of *Pollack et al.* [1993] into our coupled ice sheet model was found to produce excessively warm basal temperatures. Given the few available constraints, we chose to apply a series of bounded linear transformations to this heat flux map in order that the coupled model could be forced to approximately match the present-day observed basal temperatures at the three boreholes through the ice sheet from which such data is available. For the sake of simplicity and also to improve the match of the predictions of the model to RSL observations, we chose to impose much weaker gradients where there were no borehole constraints. The resultant modified heat flux map, show in Figure 6, is of course only reasonably constrained in the vicinity of the three data sites, denoted D, G, and C in Figure 6 (Dye 3, GRIP, and Camp Century, respectively).

[42] It is clear that borehole temperature data from Renland to the east, and from sites to the north and northeast and one from near the central west margin would allow us to obtain a much more highly constrained heat flux map for Greenland. It should also be mentioned that data sites near to, or in regions of, fast flow (e.g., Camp Century and Dye 3) would have more uncertainty associated with them, both due to the lack of explicit ice stream mechanics in the model and to the more poorly constrained climate forcing used to drive the model than is available from more inland sites such as GRIP.

[43] As an independent means of assessing the quality of the new heat flux map, it is worthwhile comparing computed and observed present-day surface heat fluxes. The only useful surface measurements available are from a

Table 4. Comparison of Model GrB and Observations[a]

	Obs	Grid Obs	GrB
Volume, 10^{15} m^3	2.828	2.848	3.276
h(summit), m	3232	3244	3245
H(GRIP), m	3029	2881	2963
T_b(GRIP) °C	−8.50		−9.24
H(Dye 3), m	2037	1859	1788
T_b(Dye 3), °C	−13.2		−13.3
H(C. Cent.), m	1387	1291	1352
T_b(C. Cent.), °C	−13.0		−14.7
H(NGRIP), m	~3100	3019	2930
T_b(NGRIP), °C	~−2.5		−7.47
h(NGRIP), m	~3000	2974	2900

[a]Included are both direct observations (Obs) and values from observational data sets gridded to the model grid (Grid Obs).

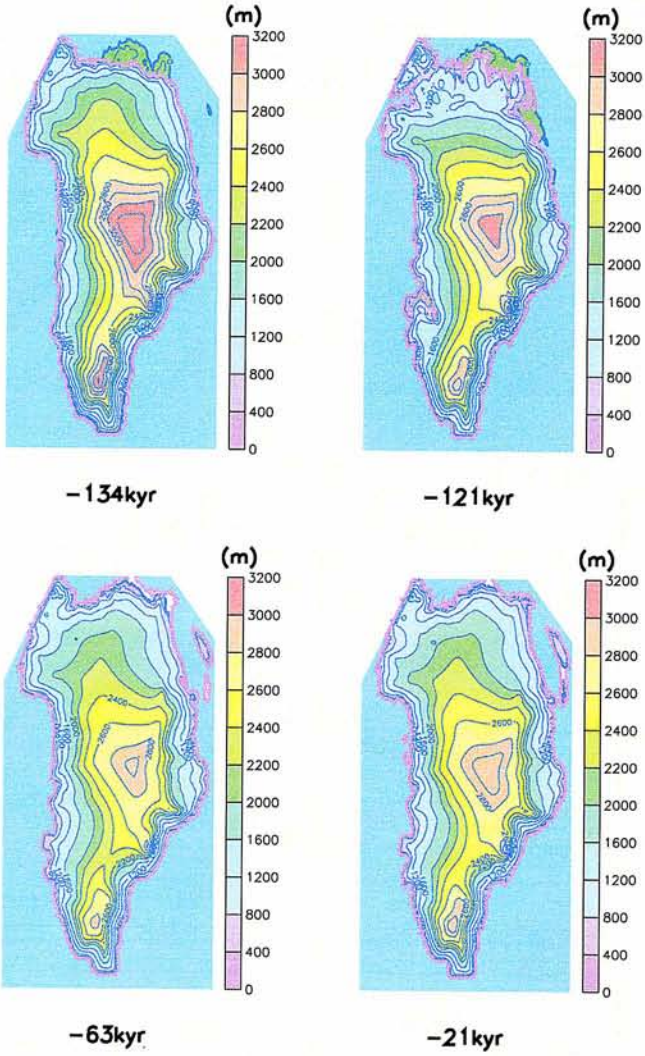

Figure 5. Snapshots from the baseline GrB model evolution of the Greenland surface topography with the contemporaneous modeled ice margin shown in violet.

series of boreholes in the Precambrian shield near the southern coastline of Greenland at Ivigtut and Ilimaussaq [*Sass et al.*, 1972] denoted Iv and Il, respectively, in Figure 6. The respective measured values of 43 and 36 mW m^{-2} are uncorrected for thermal perturbations from past ice cover. For model GrB, the present-day surface heat flows at these respective sites are 13 and 40 mW m^{-2}, a reasonably close match for Ilimaussaq but definitely not for Ivigtut. Understanding the source of such a large difference in modeled present-day surface heat flux between two proximal sites can help elucidate the source of the model-observation misfit at Ivigtut. The input deep geothermal heat flux for the two sites, 41 and 44 mW m^{-2}, respectively, are clearly not the source of the 27 mW m^{-2} difference between the modeled present-day surface fluxes. As demonstrated by *Tarasov and Peltier* [2002], who show ice thickness fields for 10 and 9 ka, both sites become ice-free at about the same time in the model (between 10 and 9.5 ka). Furthermore, both sites maintain surface elevations within approximately 200 m of each other, at least post-LGM. Climate forcing is therefore apparently not the source of the difference. Rather, the difference between the predicted heat flows is most probably due to the factor of 2 to 6 contrast in ice velocities between the two sites and the associated >12°C difference in basal temperature that existed prior to onset of the ice-free state (not shown). The higher ice velocity at Ilimaussaq resulted in increased heat advection from upstream basal ice and increased deformation heating. Throughout most of the glacial cycle, basal ice at Ilimaussaq was at the pressure-melting point, thereby allowing basal sliding with resultant surface velocities of up 310 m yr^{-1} at 10 ka. Ivigtut, on the other hand, never experiences basal sliding in the model, and basal temperatures were approximately −20°C at LGM and −11°C just before deglaciation. Near or above 0°C surface temperatures throughout the Holocene thereby resulted in a significant negative (i.e., downward) surface heat flux during the mid-Holocene.

[44] These differences between the model and observationally determined present-day heat flux values for the two sites suggest that there is insufficient model ice velocity around the Ivigtut site. This is corroborated by the enhanced Holocene forcing in the whole southwest region of Greenland required to obtain a reasonable match between model and observed RSL histories as discussed by *Tarasov and Peltier* [2002]. Though the forcing employed in this case has enhanced regional Holocene warming, it is clear that part or all of this forcing could be making up for the lack of explicit ice stream mechanics in the model. Increased ice velocities could result from an increased geothermal heat flux, however model tuning favors relatively low geothermal heat flux in the south. Though other factors likely play a role, ice thickness in the southern dome region is generally less than observed and an increase in deep geothermal heat flux would only further exacerbate this discrepancy.

[45] Partial corroboration of the northeast gradient in the deep geothermal heat flux follows from comparison of the observed and model predicted surface velocity field of the ice sheet. In a comparison with both direct and indirect measurements of surface velocity, *Bamber et al.* [2000] find that a 3-D thermomechanical ice sheet model, using a spatially constant geothermal heat flux, underestimates velocities near the northern margin and overestimates velocities in the southern margin. Increased geothermal fluxes would tend to increase local velocities and therefore the spatial gradients in the geothermal heat flux map presented herein should allow a better model match to observed velocity fields. In fact, model GrB matches to within one grid point, eight of the 10 direct (i.e., GPS based) surface velocity measurements listed by *Bamber et al.* [2000]. This has been fully discussed by *Tarasov and Peltier* [2002]. The two discrepant sites were situated around Jakobshavns Isfjord, where the very high observed velocity gradients would be difficult to capture in a model of only moderate spatial resolution. Given that model GrB overestimates near margin ice thickness in the north-northwest and east-northeast [*Tarasov and Peltier*, 2002], it is quite possible that a much stronger northeast gradient is required for the areas covered by our geothermal heat flux map that lacked borehole constraints. However, the model will require better representation of fast flow processes in order to disentangle impacts of geothermal heat flux variations and ice streams.